Chapter 5
Magneto-Plasmonic Nanoparticles

César de Julián Fernández and Francesco Pineider

Abstract Magnetoplasmonics nanoparticles encompass in a single nano-entity all the rich science and promising applications of the plasmonics and magnetic nanoworlds. The difficult liaison and a certain incompatibility between plasmonics and magnetic phenomena, due to the different chemical-physical origins and supporting materials, are overcome thanks to the design and synthesis of novel nanostructures. The variations of properties, interactions and synergies of both phenomena and materials demonstrate how rich and surprising the matter is at nanoscale and the promising applications. In fact, we show how not only light and magnetism can interplay but also other phenomena like forces, heat, electric field and chemical interactions, between others, can show synergism. Magnetoplasmonic systems are excellent benchmark materials to develop and investigate multi-responsive multifunctional nanosystems that now are required in an increasing number of technologies, such as biomedicine, pharmacy, catalysis, optoelectronics and data storage.

5.1 Introduction

Magneto-plasmonics (MPs) is new concept of multifunctional nanomaterials exhibiting simultaneously plasmonic and magnetic phenomena. MPs combine and intertwine two separated materials science worlds, magnetism and photonics, at the nanoscale. In general, MP materials are composed by the materials that originate each phenomenon: plasmonic materials are elements constituted by mainly Au, Ag and Cu while magnetic materials are formed by *3d* metals and their oxides. Since plasmonic phenomena mainly manifest in the nanometric range, also MP materials are designed in this dimension range. At this scale, both plasmonics and magnetic

C. de Julián Fernández (✉)
Institute of Materials for Electronics and Magnetism, Italian Research Council, Parma, Italy
e-mail: cesar.dejulian@imem.cnr.it

F. Pineider
Department of Chemistry and Industrial Chemistry, University of Pisa, Pisa, Italy
e-mail: francesco.pineider@unipi.it

D. Peddis et al. (eds.), *New Trends in Nanoparticle Magnetism*,
Springer Series in Materials Science 308,
https://doi.org/10.1007/978-3-030-60473-8_5

materials exhibit a rich phenomenology correlated to size and surface effects that will be present also in the MPs nanomaterials. In addition to size effects, the properties of the MP nanoparticles are affected by structural and electronic correlations between the two types of elements or materials, the final properties being different than those of bare magnetic or plasmonic materials and hence giving rise to novel properties. Moreover, very promising new phenomena and applications appear due to the synergy between the two moieties. For these reasons, nowadays MP materials are object of intense investigation in materials science. In addition, these new materials have given rise to the development of novel applications of each class of material—photonics for plasmonics and recording for magnetism—and multifunctional applications in the fields in which both materials are promising like in biomedicine and catalysis [1–5].

Focusing on the term *plasmonics*, [1, 6] this describes optical phenomena produced by the excitation of collective electron oscillations, the surface plasmon resonances (SPR), that are induced by an electromagnetic field (EMF) propagating in a metal/dielectric interface. In the case of nanoparticles, the SPR is denominated localized surface plasmon resonance (LSPR), but SPR can be generated in other morphologies as disks, thin films (propagating SPR), holes, gratings and a wide number of structures [1–9]. Plasmonics opens in photonics the possibility of new ways to manipulate the light, new optical properties of matter, and the possibility of engineering light at the nanoscale [1–3].

The possibility of obtaining a single material with both strong plasmonic and magnetic properties is nowadays an unsolved issue. Plasmonic phenomena require the presence of free electrons, hence metals with a partially-filled *s*-band at the Fermi level [1, 8–10]. On the opposite, magnetism is mainly correlated to bound electrons in the *d* and *f* bands [11]. Hence both properties are correlated to materials with very different electronic features that are not compatible in the same electronic structure. In fact, the main plasmonic materials, Au and Ag, are diamagnetic while most of magnetic metals like Fe, Co and Ni exhibit weak plasmon resonances.

Figure 5.1 shows a selection of the wide variety of MP NPs that have been grown so far [12–15]. Between all, magnetic metal NPs should be most simple MPs system that can exhibit magnetic and plasmonic properties simultaneously in a single entity. Also NPs composed by a solid solution of the magnetic and plasmonic elements—like AuFe, AgFe, AgCo should be good candidates. However, as we will discuss later, the electronic structure of the single phase and the solid-solution NPs is such that one or both plasmonic and magnetic properties are typically damped. The design of hetero-structures in which plasmonic and magnetic moieties are separated but in direct physical and electronic contact is a second approach to design MP systems. A wide variety of morphologies have been created, such as core@shell (CS), flowers, heterodimers (HSs), hybrid-cigars, stars, nanodomes, etc. These MP systems have nanometric dimension, hence the size and surface effects have a key role in their properties. Their sizes are smaller or of the order of the characteristic lengths of plasmonic and magnetic phenomena, i.e. visible light wavelength, electron mean free path and domain wall length. Then, the magnetic and plasmonic properties should be affected

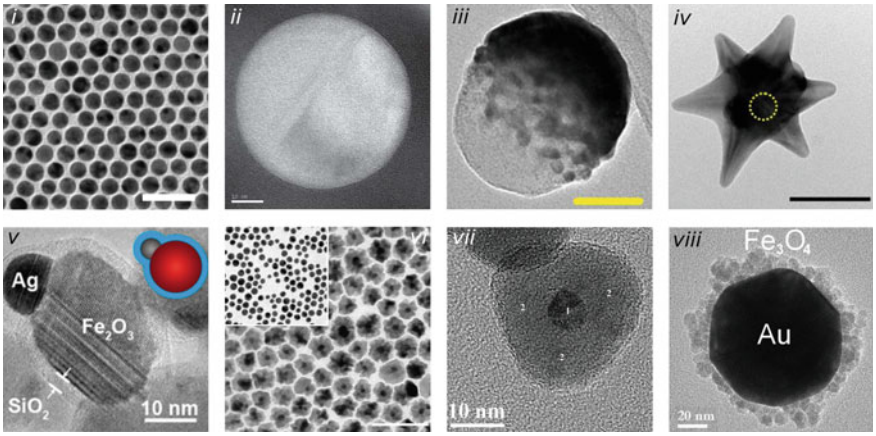

Fig. 5.1 Transmission Electron Microscopy (TEM) images of a variety of MP nanostructures. **i** Bare Au NPs, scale bar is 40 nm [229] (Adapted with permission from [229]. Copyright (2013) American Chemical Society). **ii** Solid solution AuFe NP, Energy Field TEM mapping at the Au N-edge (83 eV) [27] Adapted by permission of The Royal Society of Chemistry. **iii** MP nanodome with 20 nm Fe core and 20 nm Au layer, the scale bar 50 nm [135] (Adapted by permission from Elsevier). **iv** Au nanostar with superparamagnetic core outlined by the dashed circle, the scale bar is 50 nm [175]. Adapted with permission from [175]. Copyright (2009) American Chemical Society. **v** Asymetric SiO_2-coated Ag-Fe_2O_3 HD [165]. Adapted with permission from [165]. Copyright (2013) American Chemical Society. **vi** Flower-like Au@iron-oxide CS NPs. Inset Au nanocrystals seeds, scale bar is 100 nm [89]. Adapted with permission from [89]. Copyright (2012) American Chemical Society. **vii** Au@iron-oxide CS NPs [81]. Adapted by permission of The Royal Society of Chemistry. **viii** Fe_3O_4-decorated Au NPs [124] Adapted with permission from [124]. Copyright (2013) American Chemical Society

and correlated considering different coupling mechanisms: interparticle electromagnetic or magnetic dipolar interactions and intraparticle chemical, structural and electronic couplings. In fact, some studies show that the plasmonic and magnetic properties of the MP systems are different from the independent plasmonic and magnetic moieties. In addition, the MP properties of this variety of nanostructures can be correlated to their morphology but also to the mechanisms of magnetic and optical coupling. In the first section of this chapter, we will discuss the way in which plasmonic and magnetic moieties are correlated in the different morphologies developed so far. In the second part, their possible applications will be presented. In the third section, we will discuss the specific case of the plasmon assisted magneto-optical phenomena and finally discuss on the perspectives of these materials.

5.2 Optical and Magnetic Properties of MP Nanoparticles

Let us consider first the LSPR in small plasmonic and magnetic single metallic particles. The simplest description of the LSPR corresponds to the Mie model, [1,

6–8] that solves Maxwell's equations of propagation of an electromagnetic field in a metallic sphere. Plasmon resonances can correspond to single-mode or multi-mode electronic excitations that modify the scattering and the attenuation of the light [1, 6–8]. In the case of nanoparticles with sizes below 30 nm-case that will be mainly discussed here—the wavelength of the exciting light (for Vis or nIR light, between 275 and 1000 nm) is larger than the particle size. Considering other conditions such as the absence of interparticle electrical interactions and that the medium is a pure, non-lossy (i.e. non-absorbing) dielectric, the electrodynamic behavior of a particle can be described as that of a dipole in which the phase of the incoming electromagnetic field is constant over the particle volume [1, 3, 8]. The absorption spectrum is determined by the attenuation phenomenon (scattering is negligible, thus extinction ≈ absorption) at which corresponds an absorption cross section σ_{ext} of:

$$\sigma_{ext} = \frac{24\pi^2 R^3 \varepsilon_m^{3/2}}{\lambda} \frac{\varepsilon_2}{(\varepsilon_1 + 2\varepsilon_m)^2 + \varepsilon_2^2} \tag{5.1}$$

Absorption depends on the nanoparticle radius, R, on the light wavelength, λ, on the dielectric constant of the medium, ε_m, and on the real and the complex dielectric constant of the metal of the nanoparticle, $\varepsilon_1 + i\varepsilon_2$, The plasmonic resonance occurs at the wavelength λ_p at which when the denominator of the second part of 5.1 is zero or minimum, denominated Mie resonant conditions:

$$\left(\varepsilon_1(\lambda_p) + 2\varepsilon_m\right)^2 + \varepsilon_2^2(\lambda_p) = 0 \tag{5.2}$$

The calculated σ_{ext} using 5.1 of selected plasmonic and magnetic nanoparticles with a $R = 5$ nm dispersed in silica medium ($\varepsilon_m = 2.16$) are represented in Fig. 5.2c, d.

Figure 5.2a and b represent respectively the wavelength dependence of the dielectric constants of the main plasmonic materials, Au and Ag, as well as the Ni of some magnetic metals and alloys: Ni, Co, Fe, $Fe_{80}Ni_{20}$ (Permalloy) and FePt (in L_{10} structure). Optical data were obtained from [16–18]. As can be seen in Fig. 5.2c, both Au and Ag exhibit a very strong increase of absorption at the plasmonic resonance, followed by a decrease of the absorption in the IR range. In comparison, the SPR peak of the Ni is quite weak (observe that Fig. 5.2c is in powers of ten scale), while absorption is almost constant toward the IR spectral region. Figure 5.2d shows that Fe and FePt exhibit broader SPR peaks, while the SPR of Co and $Fe_{80}Ni_{20}$ should be at lower wavelength. The differences in strength and energy for the excitation of the SPR between the plasmonic and magnetic materials can be correlated to their electronic structures. In first instance, considering the dielectric functions of the metals in terms of the Drude-Sommerfeld model of free electrons [1, 9, 20], plasmon resonance of magnetic metals should be strongly damped and blue shifted with respect to the plasmonic metals. This is due to the larger density of electrons at the Fermi level [20] that shift the bulk plasmon resonance to high energies and to higher relaxation times [9, 10] of the magnetic metals. A more realistic approach to describe the dielectric

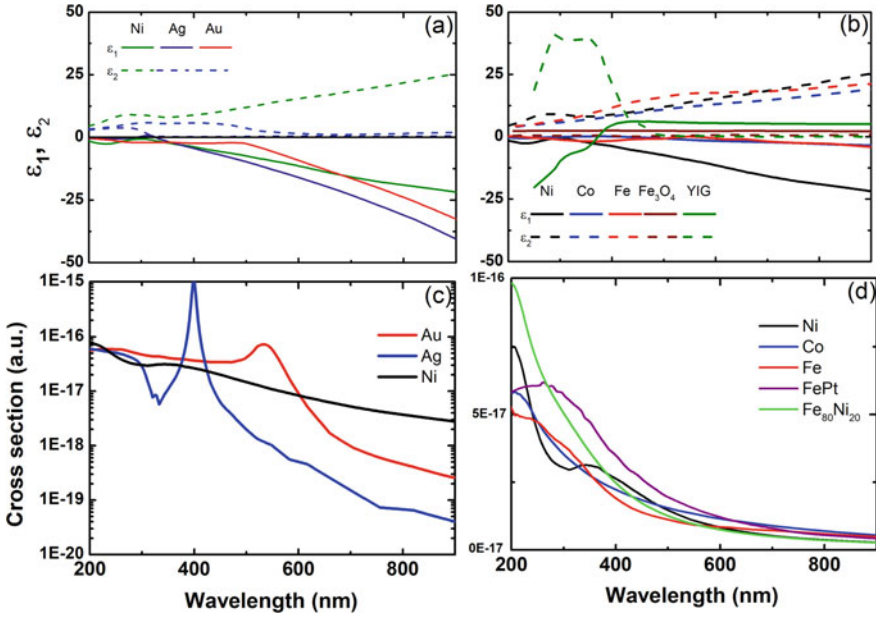

Fig. 5.2 **a** Dielectric constants of Au, Ag, Ni, **b** dielectric constants of Ni, Co and Fe and Fe_3O_4 (magnetite) and YIG. Plasmon cross sections calculated with 5.1 for 5 nm particles of **c** Au, Ag, Ni and **d** Ni, Co, Fe, FePt and $Fe_{80}Ni_{20}$

function of metals takes into account the contribution of both intraband and interband optical transitions. Intraband transitions occur in the conduction band and they can be described in terms of free electron model [1, 8–10]. They are directly involved in the SPR excitation. Interband transitions occur between different bands (like *d* and *p*) and the conduction band. In metallic magnetic materials the localized *3d* band reaches the Fermi level. This increases the probability of interband transitions to occur, giving rise to an increase of non-radiative relaxation processes. Spin–orbit coupling, characteristic also of *3d* electrons, determines further relaxation processes that damp free electron oscillations. The overlapping of the interband and the intraband transitions in correspondence of the SPR of magnetic metals gives rise to the SPR damping. In fact, no overlapping of the two type of transitions is present at the SPR of Ag, while in Au overlapping occurs only at high energy region of the SPR. In magnetic metals, the interband transitions are allowed in all the Vis and nIR spectrum [9, 21, 22]. Then the optical absorption (mainly represented by ε_2) of the magnetic metals is larger than that of the Au and Ag. This explains the damping of plasmon resonance in magnetic nanomaterials. Different experimental studies confirm qualitatively but not quantitatively the plasmonic phenomenology of magnetic metallic nanoparticles [21–24]. In fact, this description does not include a realistic contribution of size and surface effects that affect critically the electronic structure of magnetic metals and, even more simply, effects as oxidation or morphology.

An alternative simple approach to develop MP materials is using single particles composed by a solid solution of magnetic and plasmonic elements. The most important plasmonic elements, the Ag and Au, are poorly soluble in Fe and Co in the bulk, but their alloying has been experimentally demonstrated in nanoparticles [25–29]. Size and surface effects allow overcoming the thermodynamic equilibrium immiscibility [29–31] but the synthesis of alloy MP NPs is nowadays a challenge. As a consequence of the mixing of both elements, electronic hybridization occurs between the *5d6s* bands (for gold) and the *3d4s* bands of the plasmonic and magnetic metals, respectively, which gives rise to larger electronic densities at Fermi level and a broad spectral overlap of the inter and intraband transitions [26, 27, 29]. This leads to a significant damping of the plasmon resonance. At difference with single metal and hybrid nanostructures, the SPR of the alloys can either blue shift or red shift [29] depending on the metal composition. The optical properties of these alloys are different than those corresponding to the weighted combination of the constants of the containing elements, as demonstrated by Amendola et al. [27], who simulated the SPR spectrum of AuFe nanoparticles first considering the dielectric properties measured from AuFe films, then using theoretical values obtained combining elemental weighted dielectric constants of the Au and Fe. Significantly better agreement with the experiment was found using the former set of optical constants.

A second class of systems are the hybrid heterostructures constituted by a plasmonic and a magnetic moiety that are in direct contact. In this case the optical properties of the two moieties are intertwined by their proximity (dipolar fields), but also influenced by their mutual structural arrangement (epitaxy) and electronic hybridization at the contact interface [13, 31–36]. In general the plasmonic properties depend critically on the geometry and the materials that are selected. When the magnetic moiety is metallic, the LSPRs of the two moieties could be excited separately, since they are separated in energy. However, the SPR of the plasmonic moiety can be damped by the absorption of the counterpart (Fig. 5.3v), but also electronic excitations coupling between the two moieties can occur [37–41]. For instance, Sachan et al. [40] employed Energy Electron Loss experiments to observe locally the plasmonic excitation of the two moieties of CoFe–Ag HDs (Fig. 5.3 **iii**). They determined that both moieties exhibit distinct LSPR modes that are split in energy, the LSPR of the magnetic moiety being red shifted with respect to the one of Ag. Interestingly, isolated CoFe NPs do not exhibit LSPR. Moreover, a plasmon resonance was observed at the CoFe–Ag interface corresponding to a hybridized state. In the case that the magnetic part is an oxide, this material behaves as a dielectric medium (i.e. real part of $\varepsilon_m > 1$) with also large absorption ($\varepsilon_2 > 2$). See for example, in Fig. 5.2 the dielectric functions of the most investigated oxide, the magnetite (Fe_3O_4), and the promising oxide Yttrium iron garnet (YIG, $Y_3Fe_5O_{12}$) [42, 43]. Regarding morphology, in the case that the plasmonic nanoparticles are surrounded totally (in CS NPs) or partially (as in HDs) by the oxide, plasmon resonance could be analyzed by using a mean field approach (the Maxwell–Garnett, MG, model, for example) considering an absorbent medium or a multilayer structure [35, 44, 45]. As can be seen in Fig. 5.3**iv**, both in CS and HD morphologies, plasmon resonance

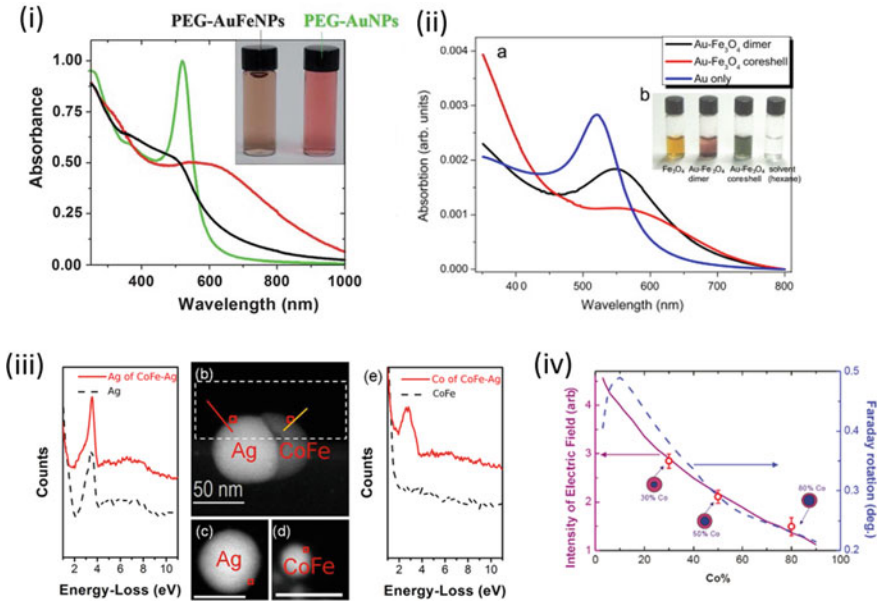

Fig. 5.3 **i** Optical spectra of AuFeNPs in ethanol (red line), of PEG–AuFeNPs in water (black line) and of PEG coated AuNPs (green line). Inset, PEG–AuFeNPs in water are reddish in color (left), different from the purple color of pure AuNPs (right) [27] (Reproduced from [27], with the permission of the Royal Society of Chemistry). **ii** Optical spectra of Au, Au–Fe_3O4 dimer and core–shell NPs; and b image of Fe_3O_4 and Au–Fe_3O_4 HNP's suspensions in hexane [160] (Reprinted from [160] with permission from Elsevier). **iiia** Experimental EELS spectra from the surface of the Ag region in a CoFe–Ag HDs NP (solid line) and isolated Ag NP (dashed line). HAADF image of **b** a CoFe–Ag HD NP, **c** an isolated Ag NP, and **d** an isolated CoFe NP. **e** Experimental EELS spectra from the surface of the CoFe region in a CoFe–Ag NP (solid line) and isolated CoFe NP (dashed line). The spectra were taken from the regions marked by square-boxes in the respective NPs. The scale bar for each HAADF image is 50 nm [40] (Reprinted from [40] with permission of the American Chemical Society). **iv** Calculated intensity of the electric field within the Co core in Co–Ag core–shell nanoparticles at resonance (continuous violet line) and maximum Faraday rotation of Co–Ag nanoparticles embedded in oil ($n = 1.5018$) (dashed blue line) as a function of the Co concentration [38] (Reprinted from [38] with permission of the American Chemical Society)

is red shifted and broadened, depending on the relative sizes of the two components. In the case of the HDs, the spectrum is the convolution of all the optical absorption spectra corresponding to all the different orientations of the MP couples respect to the propagation of light [46, 47]. The CS NPs constituted by a plasmonic shell is a different case. In general, a plasmonic crown exhibits two plasmonic modes at lower and higher energies than the plasmon resonance of the particle [39, 40, 48–50]. Including the magnetic dielectric core, both resonances are weaker and red shifted [37, 50]. Often however, the plasmonic shell is not constituted by a continuous shell but by packed plasmonic nanoparticles (Fig. 5.1h). In this morphology multimodal resonances due to interparticle dipolar interactions give rise also to the broadening of the absorption and to scattering processes. Finally, in the case that the magnetic shell

is metallic several studies show that these CS structures exhibit a single plasmonic peak that is red shifted and broader as the percentage of magnetic moiety is larger but also blue shift by modifying the size of the magnetic moiety [38]. The study by López-Ortega et al. [51] obtains a reasonable agreement of the plasmonic properties of Ag@CoFe CS with the simulations.

Previous discussions on the plasmonic properties of the hybrid systems considered a static description of the plasmon resonance, i.e. the solution of Maxwell'equations of the system. However, the dynamics of the plasmons needs also to be considered [52]. Only few different pump and probe studies [53–56] have been performed on Au–Fe oxide HDs and other morphologies, showing that the plasmon resonance is characterized by a faster electron relaxation process than that of bare Au NPs. Considering the previous described experiments on magnetic metal-plasmonic heterostructures (CoFe–Ag [38] and Ag@CoFe [51]), the hypothesis of a charge-transfer process from the plasmonic to the magnetic moiety can be proposed. Cosmin et al. [56], in contrast, proposed that the observed relaxation is due to the spill-out of electron density from gold electron at the gold/magnetic interface excluding a charge transfer mechanism. Further studies are required considering a controlled interface and chemical states of the magnetic oxide.

Composites or mixtures of isolated magnetic and plasmonic particles are the simplest MP systems. A large variety of materials have been synthesized: micro and nano capsules containing a mixture of the two classes of NPs [35]; capsules containing only one kind of nanomaterial, magnetic for example, that are decorated by the plasmonic counterpart [57, 58]; multilayers or onion-like particles in which plasmonic and magnetic moieties are separated by a dielectric layer like SiO_2 or TiO_2 [41, 59–66]. MP effects have been investigated even in mixtures or simple solutions containing the two types of NPs [67, 68]. In all these cases, the interparticle dipolar electromagnetic interactions and the absorption of the magnetic NPs determine the changes of the plasmonic resonance respect to bare plasmonic nanoparticles. Depending on the interparticle distance, the geometry of the particles and the magnetic/plasmonic nanoparticle concentration ratio, the coupling can have different strength. In very diluted systems the dielectric contribution of the magnetic moiety could be included in the term of the dielectric medium (ε_m) using a mean-field model [68, 69]. However, SPR should be calculated considering that the medium surrounding the plasmonic particles is absorbent [69–71]. A red shift and damping of the LSPR is expected as previously discussed. If interparticle distance is small (nanometers), strong confinement of the EMF occurs, and the so called "hot spots", can be present even between plasmonic and metallic magnetic nanoparticles [72, 73]. This can give rise to blue shift of the LSPR. Finally, superstructures composed by networks of the two classes of materials have been also synthesized [74, 75].

Also magnetic properties of the MP structures appear different compared to equivalent bare magnetic particles, even if plasmonic materials are diamagnetic. In first instance, the hybrid nature of MP structures determines that the growth mechanism is different to that of bare magnetic nanoparticles. For example, the synthesis of hybrid structures like CS and HDs requires a two-step process in which heteronucleation

and particle growth are involved [13, 33, 35, 44]. Crystal growth, shape and composition of the magnetic moiety can be different than bare magnetic NPs. While most studies compare bare nanoparticles with hybrid ones, in which the nucleation process is different, recent studies [78–81] have compared hybrid systems with the corresponding NPs or hollow NPs obtained after the elimination of the plasmonic moiety. Even if the morphology is similar, the two nanomaterials exhibit different magnetic properties, such as saturation magnetization and hysteresis [81]. This demonstrates the critical role in the magnetic properties of the plasmonic-magnetic interface.

More deeply investigated cases correspond to heterostructures as CS nanoparticles and HDs in which Ag and Au are combined with Fe oxide. The first effect is the modification of the magnetization of the magnetic moiety, consisting in a strong decrease of saturation magnetization of Fe_3O_4 in comparison to the bare nanoparticles. This decrease is typically correlated to the presence of a magnetic disordered layer, called dead layer, at the free surface or at the Au-interface of the magnetic moiety [45, 82–87]. In the case of CS the presence of antiferromagnetic phase boundaries in the intergranular regions of the multigrain or petals of Fe_3O_4 can also give rise to a decrease of the magnetization [61, 88]. In addition, the presence of an antiferromagnetic FeO wustite layer in the interface region between the Fe_3O_4 and Au moieties could also cause of the decrease of magnetization [61, 89, 90]. However, such behavior is not always observed as in some studies the specific magnetization is near the bulk value (80–90 emu/g), [91–93] suggesting the above proposed problem could be overcome. Further studies on the physico-chemical properties and chemical stability of these structures are required.

A significant question that illustrates the complexity of the magnetic order in hybrid system is the magnetic observation of the Verwey temperature. This is a specific fingerprint of magnetite, Fe_3O_4, not present in other Fe oxides, which corresponds to a metal-to-insulator transition around 120 K. The change of the electric nature of the Fe_3O_4 at this transition corresponds also with changes in the magnetic and optical properties of the oxide and hence plasmonic coupling features in a hybrid system could be influenced. In many studies, including both HDs and CS [81, 89, 93–95] structures the Verwey transition is observed at or below the bulk temperature value, while in other cases it is absent [45, 61, 85, 87, 96, 97]. The absence of this transition could be a fingerprint of the size effects in the oxide. However, changes in the stoichiometry or the partial oxidation of the Fe_3O_4, composed of Fe^{2+} and Fe^{3+}, to maghemite (γ-Fe_2O_3) or other oxides composed of only Fe^{3+} are more possibly the origin of these changes.

MP hybrid nanostructures exhibit also differences in the reversal process mechanism of the magnetization. In principle, most of the investigated MPs have the magnetic moieties with a dimension below the 20–30 nm, being near or below the single domain range [11]. In such case, the dominant mechanism of reversal of the magnetization is the coherent rotation of all the spins. The hysteresis loops, described by the Stoner-Wohlfarth model [11, 98], should have open loops with maximum coercive field correlated to the anisotropy field of the material. However, local and global surface and size effects determine mainly the reversal process and all the magnetic properties of the magnetic particles [11, 98, 99]. In addition, thermal

activation processes are dominant [98] and the superparamagnetic effect occurs at room temperature. This behavior has been reported in a wide number of works investigating Au–Fe_3O_4 heterodimers and Ag–Fe_3O_4 [45, 89, 93–97, 100]. The blocking temperature, i.e. the threshold between the blocked and superparamagnetic regimes, is determined by the size distribution of the particles, their magnetic anisotropy, as well as the magnetic interparticle interactions. HDs and CS NPs appear to exhibit different behavior [95, 96, 101]. In the case of HDs, some works [85, 87, 90] have shown that the magnetic moiety exhibits a spin-glass behavior due to the spin-disorder in the structure. Different is the case of the CS NPs [96, 100, 101], if the shell is magnetic and depending on the morphology of this shell—continuous shell or discontinuous layer of particles—the reversal process could take place by incoherent rotation modes or by the dipolar competition of the particles. Here, in addition to the spin-glass behavior, also exchange bias effects have been observed [87, 90, 93] even if the presence of an antiferromagnetic material counterpart, necessary for the exchange bias effect, was not detected. Chandra et al. [85] propose this behavior is possible in the Au@Fe_3O_4 CS NPs due to the presence of inner or intergranular spin disordered regions. On the other hand, Zhu et al. [87] propose that the exchange bias is due to the coupling of weak magnetic layer at the Au–Fe_3O_4 interface and the Fe_3O_4 overlayer. However, these effects are not present in all the investigated structures: other studies [89, 102] show the classical superparamagnetic behavior in which interparticle interactions are dominant even if magnetic moiety is composed by ferromagnetic (Fe_3O_4 or γ-Fe_2O_3) and antiferromagnetic (α-Fe_2O_3) phases.

The magnetic properties of alloy-based MP nanoparticles, that combine magnetic and non-magnetic elements, are completely different to those of the hybrid family. As previously mentioned, the formation of this type of alloys is not straightforward, but it is even more difficult to obtain magnetic properties at room temperature. The out-of-equilibrium nature of nanomaterials allows the growth of these alloys, but also other possible morphologies, such as segregated particles or inhomogeneous mixtures, are possible. On the other hand, the solid solution of non-magnetic and magnetic elements gives rise to the decrease of the magnetic moment of the magnetic elements resulting in the decrease of the total magnetization of the particle and the weakening of exchange interactions with the consequent decrease of the Curie temperature. In a few alloys, for example NiCu [103] or FeCuPt [104] alloys, the solid solution of the two element is possible and the magnetization and the Curie temperature decrease (non-linearly) as the non-magnetic content increases. In the case of AuFe [105–107] and AgCo [108, 109] solid solutions, in addition to this evolution, also spin-glass and diamagnetic behaviors can occur for the large content of non-magnetic elements. In fact, in these cases the decrease of the magnetization and One relevant point is thatthe Curie temperature is due to the decrease of the direct exchange interactions and the increasing role of the indirect exchange interactions (RKKY) though the *s*-bands of the non-magnetic elements. In such case the magnetic behavior can pass from ferromagnetic, to spin-glass, paramagnetic and diamagnetic, depending of the non-magnetic content but also on the temperature.

The discussions above show that the preservation of both magnetic and plasmonic properties is possible both in hybrid and in alloy nanostructures, but a fine

control of the nanostructural and compositional features is required. On the other hand, the synergistic behavior between the two moieties has been evidenced investigating other properties and effects. The main case corresponds to the magneto-optical (MO) properties of these materials that will be discussed in the next section. Another synergistic effect is the observation of a spin and orbital moments in non-magnetic atoms of alloy-based AuFe nanoparticles [26, 27]. In fact, several studies have shown the spin polarization of the *d* and *s* bands of Au and also Ag elements when are alloyed with magnetic ones [107, 110–112]. The magnetic moment of these heavy non-magnetic elements exhibits a large orbital-to-spin ratio as expected due to their characteristic large spin–orbit coupling. Similar spin polarization of plasmonic element was observed in Au-Fe_3O_4 hybrid NPs. In this case, a charge transfer mechanism at the metal-oxide interface could give rise to the spin polarization of Au [89]. This demonstrates other paths of coupling mechanisms between the magnetic and plasmonic moieties.

5.3 General Applications of MP Nanoparticles

Let us consider first optical applications of MP nanoparticles. In principle, optical properties of MP NPs follow the same behavior of the plasmonic materials, taking into account the optical changes induced by the presence of a magnetic moiety. Even considering the expected resonance shift and spectral broadening, MP NPs exhibit the same characteristics that allow to design the color, light scattering and contrast, and optical spectral features required in several photonics and imaging applications [113–116]. The modification of plasmon resonance under the variation of the environment—a key concept for refractometric sensing devices—has been shown [117–120]. The strong localization and confinement of light at the SPR, giving rise to modification of the linear and non-linear optical properties of the capping molecules or materials is also possible. This is the working principle of many optoelectronics, sensing and monitoring applications. In particular, Surface-enhanced Raman scattering (SERS) spectroscopy, a spectroscopic technique that uses the plasmon-induced enhancement of Raman signal to detect a wide variety molecules and compounds, have been demonstrated both in hybrid MPs systems [121–126] as well in alloy-based MPs structures [127–129]. Photo-thermal effects were also demonstrated in MP nanostructures. This consists in the generation of heat by NPs due to the excitation of the LSPR and is a well-established subject in applications concerning nanoparticles in biomedicine [130–136] and catalysis [137]. One of the features that has brought the interest for MP nanostructures is the possibility to tune the SPR down to the n-IR region. Nowadays, this is a researched property for photonics in telecommunications and biomedical applications. In telecommunications, the scope is the reduction of losses and the coupling with telecom lasers [9, 10]. The employment of plasmonic effects and techniques under in-vivo conditions for biomedicine applications is limited by the complete absorption of light in the visible range by the skin and other bio-tissues [138, 139]. MP NPs can be prepared to exhibit the SPR in the

n-IR region where the first optical window, at around 700–800 nm, is present. This allows the development of in-vivo plasmon-assisted imaging techniques, but also for the application of photo-thermal therapy [130, 132, 134, 135] for deeper tissues.

Besides their plasmonic properties, gold nanostructures are investigated in biomedicine for their low cytotoxicity, biocompatibility and inertness [4, 93, 139, 140] and/or the established and wide possibilities of functionalization of Au surfaces with large number of molecules and materials [4, 5, 139, 141, 142]. The plasmonic moiety—attached to another active component—can assure the protection of the active component to chemically and biologically reactive or aggressive media. The gold moiety can cover the active component in such a way to reduce its toxicity or its release rate. Hence, plasmonic nanostructures are considered as key actuators for biomedical applications like drug delivery and genetic manipulation but also for environment sustainability [4, 8, 139, 141]. These questions are particularly important for applications in which magnetic nanoparticles are involved: except the Fe oxides (magnetite or maghemite), most of magnetic compounds are chemically oxidisable, reactive, and considered cytotoxic [140, 143, 144]. Hence the term "magnetoplasmonic" is also employed to define also hetero-nanostructures in which the magnetic moiety is covered by an Au layer or by Au NPs. Nowadays strong activity is performed in the understanding of the clearance, retention and toxicity of several MP nanostructures [145–148].

Concerning magnetic applications, MP NPs are now appealing for biomedical applications (some cases represented in Fig. 5.4), and are being considered also for catalysis and environmental applications. Like bare magnetic nanoparticles, the MP NPs can be moved and placed or concentrated in a region, tissue or on device using magnetic fields [113, 149]. These systems allow also the active particle concentration and guiding for in-vivo and in vitro biomedical applications [35, 36, 113, 133, 134, 149, 150] and improvements of concentration or separation for biomedical analysis [151–157]. They have also been employed as *contrast agents* using Nuclear Magnetic Resonance (NMR) [36, 62, 66, 157–162] and ultrasound biomedical imaging techniques [163, 164]. Several studies have demonstrated the improved relaxivity features of MP NPs, faster relaxation times (T1) than the commercial particles and promising T2 dephasing times. This has been observed both in Au–Fe_3O_4 heterostructures [157, 161, 162] and in weakly magnetic AuFe alloy-based NPs [27, 128] showing how the novel magnetic structures of these hybrid materials can improve the properties of bare magnetic particles. Finally, the heat generation of the MP NPs irradiated by radiofrequency magnetic field and its employment for cancer therapy was demonstrated [62, 81, 92, 94, 97, 121, 165–168]. The aim is to produce externally a local heating that can induce the apoptosis of cancer cells, the thermal induced release of drug or the activation or increase of efficiency of drugs. In addition, a novel approach of cancer therapy based on magnetomotive activity, mechanical or stress-induced damages produced by the rotation of the magnetic particles into the cellular target, was developed considering MP nanostructures [169, 170]. In this case the capping of Au layer of the magnetic moiety allows the surface functionalization, low cytotoxicity and it ensures the chemical and mechanical stability during the rotation or vibration of the particles into the cells.

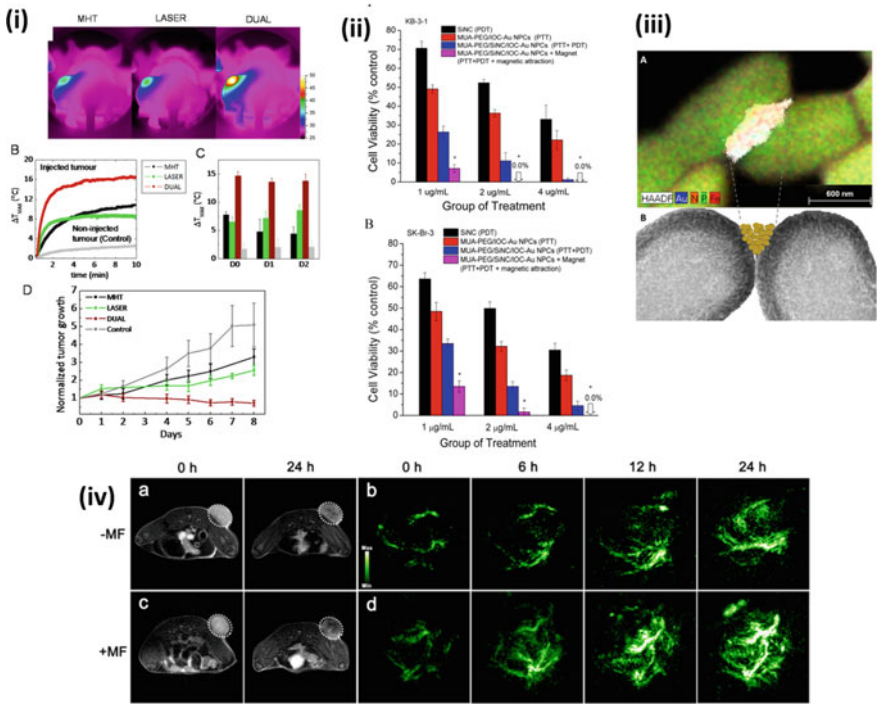

Fig. 5.4 **ia** Thermal images obtained with the IR camera in mice, after intratumoral injection of nanocubes in the left-hand tumor, and after 10 min application of magnetic hyperthermia (MHT, 110 kHz, 12 mT), NIR-laser irradiation (LASER, 808 nm at 0.3 W/cm^2), or DUAL (both effects). **b** Corresponding thermal elevation curves for all treatments and for the noninjected tumor in the DUAL condition. **c** Average final temperature increase obtained after 10 min on day 0 (1 h after injection) and 1 and 2 days after injection and for non-injected tumors. **d** Average tumor growth (groups of six tumors each in non-injected mice submitted to no treatment (Control) and in nanocube-injected mice exposed to MHT, LASER, and DUAL during the 8 days following the 3 days of treatment [183] (Reprinted from [183] with permission of the American Chemical Society). **ii** Comparison of the efficacy of different combinations of Photo-thermal therapy (PTT) with Photodynamic therapy (PDT) and magnetic attraction against KB-3-1 (**a**) and SK-BR-3 (**b**) cells using Au capped Fe oxide NPs (IOC-Au) capped with a capping layer of near-infrared absorbing photosensitizer silicon 2,3-naphthalocyannie dihydroxide (SiNC) and/or poly(ethylene glycol) (PEG) linked with 11-mercaptoundecanoic acid (MUA) [133] (Reprinted with permission from [133]. Copyright 2017 American Chemical Society). **iiia** STEM-electron dispersive energy micrograph map of colistinated FeOx/Au nanoclusters binding to A. baumannii. b Schematic of FeOx/Au nanoclusters binding to A. baumannii bacterium (STEM micrograph) [156] (Reprinted with permission from [156]. Copyright 2017 American Chemical Society). **iv** In vivo T2-weighted MR images of 4T1 tumor-bearing mice at various time points post-injection of gold nanorods @ Fe oxide core@shell particles load with doxorubicin (GNR@IOs-DOX) without (a) or with (c) magnetic tumor targeting. White circles indicate the positions of tumors. b, d In vivo Photoacustic images of the tumor sites at different time points postinjection of GNR@IOs-DOX without (b) or with (d) magnetic targeting [134] (Reprinted with permission from [134]. Copyright 2016 American Chemical Society)

Among the most appealing properties of MP NPs is the combination of magnetic and plasmonic properties and the *multifunctional approach* that can be reached with these structures. Magnetoplasmonic systems were first considered to overcome many of the limitations of plasmonic systems. MPs was one of the first concepts considered to develop "*active plasmonics*" [171], i.e., plasmonics devices which SPR, and hence the optical properties, could be manipulated externally [12, 14, 171–174]. The optical properties of the MP particles are modulated by an external magnetic field as a consequence of the change of their magneto-optical properties (see next section). Another path to modulate the optical properties is the design of asymmetric structures, as stars, in which a rotating magnetic field induces the movement (rotation) of the particles that gives rise to time-dependent changes of the reflectivity [27, 175, 176].

A second contribution of MPs concerns the improvement of the possibilities of *manipulation* of the plasmonic systems for biomedical targeting therapies (Fig. 5.4ii, iii, iv). In fact, the efficiency of plasmonic structures for drug or gene delivery, for targeting and for separation is determined by the possibilities of functionalization and anchoring to the targets [151]. Adding the possibilities of the spatial manipulation with a magnetic field gradient it is possible to improve the drug-delivery, tracking, intracellular drag update, and the particle retentivity in in-vivo applications [150, 177, 178]. In in-vitro tests and lab-on-chip applications it is possible to drag the particles, to localize and to concentrate the target molecules, genes, DNA and hence to improve sensibility of devices between other properties [153–157, 179].

Regarding the *thermal therapy* approach, both photo-thermia and magnetic hyperthermia methods can be simultaneously applied in MP NPs [35, 97, 121, 151, 180, 181]. As was previously discussed, the choice of MP structures can improve critical questions related to the employment of each class of particles in therapy, i.e. the cytotoxicity and the elimination of magnetic particles and the application of plasmon-assisted photo-thermal therapy in the NIR. In fact, photo-thermia can only be applied to targets placed at few centimeters from the skin, employing NIR radiation, while magnetic fields can be designed to reach deeper areas. Recent studies have outlined the improvement of the local thermal heating combining simultaneously the two procedures [97, 133, 180, 183] (Fig. 5.4i). Some studies indicate that the improvement is due to combination of the two thermal processes rather than to a synergistic effect [97, 182, 183].

Considering the activity of the plasmonic and magnetic moieties as probes, optical (photoacoustic, pholuminescence) and magnetic (NMR, ultrasound, magnetic, magneto-motive) imaging techniques can be combined in a *multimodalapproach* [15, 63, 65, 117, 128, 130, 134, 151, 177, 184, 185] with MPs NPs (Fig. 5.3iii, iv). Different types of imaging probes, like Vis and IR light, ultrasounds and radiofrequency (NMR), new imaging methods, like optical magneto-motive [163, 164] and magneto-optical techniques designed with MP NPs, and other clinical tests like positron emission Tomography or X-ray computed tomography [128, 179, 184–186] can be simultaneously employed to obtain images at penetration larger than the optical threshold of each probe. In addition better spatially resolved and complementary information can be obtained. Also enhanced imaging sensitivity and accuracy is

expected in such a way to get a better understanding of biomedical systems and an accurate anatomical and functional information from inside the body and in bio-tests.

MP nanostructures can be considered for *multiple theranosticapproaches* in biomedicine [187, 188] (Fig. 5.4ii). Theranostics considers the simultaneous or consecutive combination of diagnostic and therapeutic methods for a personalized, faster and efficient medical treatment. Independently, both plasmonics and magnetic nanoparticles, are considered for a theranostic approach mostly focused to cancer treatments. With MP nanoparticles, a wider range of targeting, diagnostic and therapeutic possibilities is available, as demonstrated the increasing number of studies [59, 60, 62, 131, 132, 135, 147, 178, 189–193].

5.4 Magneto-Optical Effects in MP Nanoparticles

Considering that the plasmonic phenomenon is mainly an optical effect, the direct cross-linking between the magnetism and plasmonics is the magneto-optical (MO) effect [172, 174]. This term describes a wide number of optical phenomena correlated to the interaction between light and matter in which the properties of light change after interacting with a magnetic material or any material under a magnetic field [194, 195]. In this chapter, we will discuss the main MO linear effects correlated to magnetic materials: the Faraday effect, Magnetic Circular Dichroism (MCD) and the Kerr effects. The MCD and the Kerr effect—in transverse configuration—involve changes in the light absorption, while the Faraday and Kerr effect—in longitudinal and polar configurations—give rise to the change the polarization of the light producing the change of the angle of polarization and give rise to an ellipticity. These MO effects are proportional to the magnetization of the magnetic material and hence change as a function of applied magnetic field and temperature. In fact, MO can be regarded also as a magnetometric technique that allows to measure the hysteresis loops of surfaces, films and also nanoparticles. The information on the magnetic properties coming from the MO effects depends on the penetration depth of light in matter at the specific wavelength and can range from some tens of nanometers for metals to centimeters for magnetic dielectrics (YIG, for example).

MO effects are due to optical transitions that follow the dipole selection rules i.e. requiring a change of the angular momentum of ± 1. Hence MO spectroscopy gives complementary information to other spectroscopic techniques as MO transitions can depend on crystal symmetry and spin-electronic structure, in particular concerning bands split by the Spin–Orbit (SO) coupling [194–196].

These MO effects are incorporated in the description of optical phenomena by describing the optical properties of the material with a complete dielectric tensor that includes the non-diagonal magneto-optical terms [14, 19]:

$$\varepsilon = \begin{pmatrix} \varepsilon_{xx} & \varepsilon_{xy} & \varepsilon_{xz} \\ -\varepsilon_{xy} & \varepsilon_{yy} & \varepsilon_{yz} \\ -\varepsilon_{xz} & -\varepsilon_{yz} & \varepsilon_{zz} \end{pmatrix} \tag{5.3}$$

where ε_{ii} and ε_{ij} $(i, j = x, y, z)$ compose the complex dielectric function that depend on the magnetization state in the respective directions.

The coupling of MO and plasmonic phenomena is currently being investigated in a wide number of MP morphologies, like nanoparticles, films, hollow films, gratings, disks, and more complex morphologies [14, 19, 174, 197]. NPs are probably one of the least investigated classes of MP candidates, due to the previously discussed complexity in their structure and composition. Many of the phenomena that will be discussed on the NPs have been theoretically predicted and observed in other morphologies. In particular, results on plasmonic nanodisks that also exhibit LSPR will be proposed as a reference.

In single-phase nanoparticles, the dielectric tensor of the material can be used in Mie equations to obtain the single-particle absorption and scattering cross sections; [198, 199] as an alternative, an effective medium such as the generalized Maxwell–Garnett (MG) approximation can be used to describe the system [22, 23, 200, 201]. In the case of the Faraday and MCD experiments, that are performed in transmission configuration, for optically isotropic magnetic materials, the dielectric tensor is simplified as $\varepsilon_{xx} = \varepsilon_{yy} = \varepsilon_1 + i\varepsilon_2$ and $\varepsilon_{xz} = \varepsilon_{yz} = 0$. Considering the MG equation for diluted particles the angle of plane rotation (θ) and the ellipticity (ϵ) of the polarization in the Kerr configuration is [202–204]:

$$\theta + i \in = \frac{2\varepsilon_m}{(\varepsilon_{xx} - \varepsilon_m)(\varepsilon_{xx} + 2\varepsilon_m)} \varepsilon_{xy} \tag{5.4}$$

As in the case of the 5.2, resonant conditions for the MO signal should appear as in the denominator reaches a minimum. In this case it occurs under two conditions (a) $\varepsilon_{xx} = -2\varepsilon_m$, hence to the excitation of the SPR corresponds an amplification of the MO effect and (b) $\varepsilon_{xx} = \varepsilon_m$, hence, MO amplification can occur upon a different excitation of the SPR.

Amplification of MO effects at the SPR have been observed in a wide number of single phase metallic NPs of Fe [21, 205], Ni [23] and Co [22, 24] as well as FeCo [206] and FePt [207] alloys nanoparticles, phenomenologically confirming the existence of the effect. The change of MO signal as a function of different structural factors, such as the particle size in the Fe NPs [21] and in the Co NPs [208, 209] (see Fig. 5.5i), the packing factor in Co nanoparticles [24], and the nature of the medium surrounding Co NPs [210–212], follow the behavior of the SPR. As was previously discussed, SPR in magnetic metallic NPs is blue shifted in comparison to plasmonic NPs. This is also observed in the MO spectrum, but the MO line shape can be a peak or a dispersive curve depending on type of MO effect that is measured. However, in most of these studies there is not a good agreement between the theoretical calculations and experimental MO measurements. In most of the

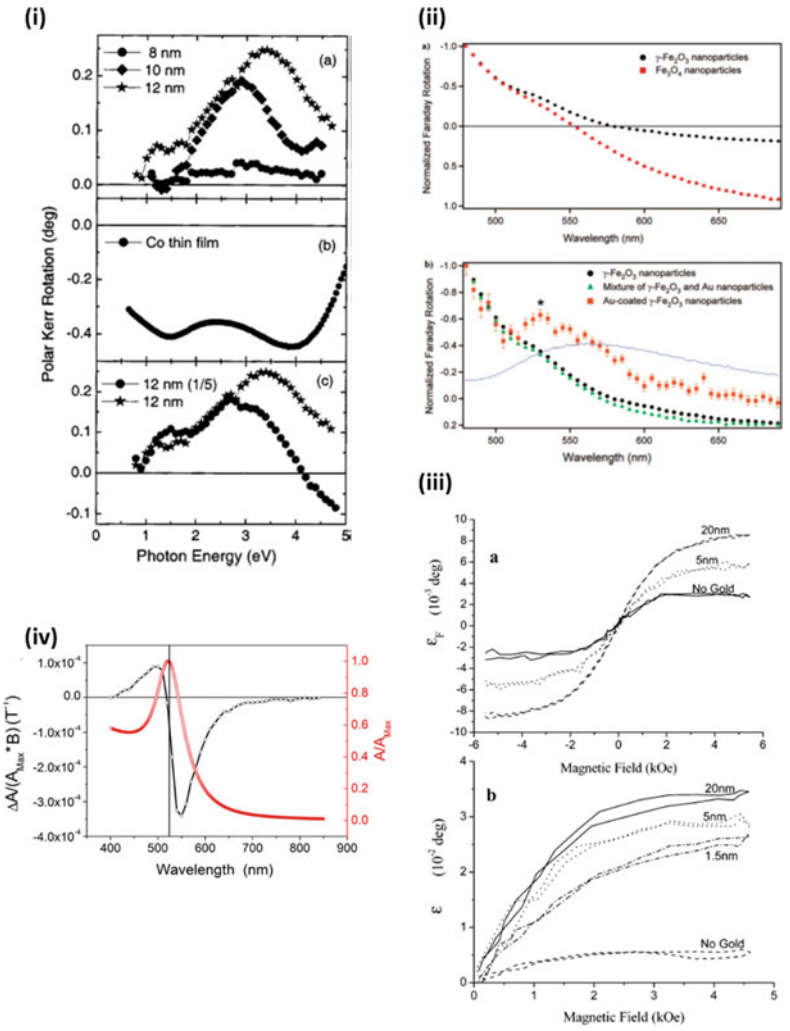

Fig. 5.5 **ia** MOKE spectra of thin films consisting of 8, 10, and 12 nm size Co particles deposited on Al substrate. **b** Co thin film reference spectrum. **c** Influence of solution dilution of the particles on the MOKE signal [208] (Reprinted from [208], with the permission of AIP Publishing). **iia** Normalized Faraday rotation spectra of γ-Fe_2O_3 and Fe_3O_4 nanoparticles. **b** Normalized Faraday rotation spectra of γ-Fe_2O_3 nanoparticles, gold-coated γ-Fe_2O_3 nanoparticles, and a mixture of γ-Fe_2O_3 and gold nanoparticles. The absorbance spectrum showing the plasmon resonance band of the gold-coated γ-Fe_2O_3 nanoparticles is indicated by the dotted blue curve [222] (Reprinted with permission from [222], Copyright 2009 American Chemical Society). **iii** Comparison between MCD magnetization curves for magnetite nanocrystal monolayers with and without a rough gold film measured in transmission (**a**) and reflection (**b**) configurations [217] (Reprinted with permission from [217], Copyright 2002 American Chemical Society). **iv** Optical absorption spectrum (red ○), and MCD (black ○) of the gold nanoparticles. Optical absorption (A) is given in normalized units at peak maximum (A/A_{Max}); dichroism (ΔA) is scaled in accordance ($\Delta A/A_{Max}$) [229] (Reprinted with permission from [229], Copyright 2009 American Chemical Society)

previous studies it has been argued that such differences come from the difficulty in accurately determining the optical and magneto-optical properties of magnetic materials composing the nanostructures, since they can be affected by oxidation processes and by surface and size effects, resulting in a dielectric tensor with can be very different from the starting bulk material, and very hard to characterize. Vlasin et al. [213] propose to take into account the diamagnetic MO contribution of the medium, to adequately perform the theoretical calculations with the MG model.

The amplification of the MO signal has been theoretically calculated with the Maxwell–Garnett effective field approximation in bimetallic CS and onion-like nanostructures [201, 214, 215] and observed in Ag@Co [38] and Ag@CoFe CS NPs [51] and Au top-capped Ni wires [216]. López-Ortega et al. [51] compares the plasmonics and MO properties of CoFe NPs to those of Ag@CoFe NPs (Fig. 5.3iv). The bare magnetic NPs do not present SPR and their MO signal is weaker than that of the MPs CS NPs that have a SPR and Faraday effects at coincident wavelength. Interestingly, the MO signal exhibits a similar shift in energy as the SPR when the surrounding medium is changed, indicating the possibility to apply the MO technique for chemical and biochemical sensors.

Wang et al. [38] investigated the evolution of the plasmon-induced MO signal of Au@Co CS NPs as function of the Co shell thickness. They observe an increase of the Faraday signal and of the SPR as Co layer was thinner even if bare Co NPs had small MO signal and no SPR. This behavior was in agreement with the simulations employing MG model confirming the expected damping of the SPR induced by the strong absorption of the magnetic component. However, the authors correlate the stronger MO activity of the CS NPs with thinner magnetic layer to an amplification effect of the EMFs induced at the LSPR. In fact, the local enhancement of the EMFs at the plasmonic resonance is a well-known and exploited optical effect that can give rise to the amplification of a wide number of optical effects. For example, Shemer et al. [217] showed that the Kerr effect in Fe_3O_4 NPs increases up to 3 times when placed in the proximity of plasmon-active rough metallic surfaces (Fig. 5.3iii). The proof of concept for this plasmon-amplified MO effect was demonstrated in composites of Au nanoparticles dispersed in garnet films [218–220]. The majority of available studies currently involve CS and HDs NPs [221–223] with magnetite (Fe_3O_4), maghemite (γ-Fe_2O_3) or spinel oxides doped with a second transition metal cation, due to the easier synthesis and their possible application in biomedicine. Jain et al. [222] reported the amplification of the Faraday signal of Au-coated maghemite nanoparticles (Fig. 5.3ii). Li et al. [221] observed an increase of the Faraday rotation and a change of its sign in Ag–$CoFe_2O_4$ HDs, but not at the SPR wavelength. In fact, the comparison between the MO properties of the bare magnetic moiety and in the hybrid nanostructures is not straightforward, due to the previously discussed magneto-structural differences between the two systems.

Several studies investigated the MO properties of mixtures of magnetic and plasmonic NPs, in which direct contact is excluded and mainly near field EMF interactions modify the MO signal. Several studies have shown the amplification [224, 225] or the reduction [68] of MO signal and the change of its sign [224], considering different interparticle distances and hence different dipolar strength. Discrete

Dipole Approximation calculations predict in Ag and $CoFe_2O_4$ packed NPs a non-monotonic dependence of the MO signal on the interparticle distance, the maximum being at 20 nm interparticle distance [226].

The overlapping of the SPR with a MO transition has been also taken into account. Campo et al. [68] investigated the effect of the SPR on the different MO transitions of $CoFe_2O_4$ NPs dispersed in a solvent with a small concentration of Au NPs (<1%). This oxide exhibits three bands associated to different interband and intraband optical transitions. The broad SPR peak of the composite overlaps with the interband charge-transfer (CT at 1.8 eV) transition and a crystal field (CF at 2.0 eV) transition of the Co^{2+} ions, which result in distinct MO spectral features. While the MO signal at the CF transition decreases, the one of the CT transitions that fully overlaps with the SPR, evolve to several weak MO transitions. On the other hand, plasmon-induced amplification of the MO signal of single-molecule magnet molecules (terbium(III) bis-phthalocianinate) deposited of Au discs was recently observed [227]. In this case the SPR of the substrate discs almost overlaps with the MO transitions related to the main absorption band of the molecule. A moderate, but very clear fivefold enhancement of the MO signal from the magnetic molecule was observed in this case.

One relevant point is that also non-magnetic plasmonic nanostructures exhibit MO effects at the SPR [203, 228, 229]. In fact, the interaction of light with free electrons in presence of a magnetic field perpendicular to the oscillating electric field of light gives rise to magneto-optical effects due to the Lorenz force [198, 230]. This results in Kerr or Faraday rotations due to the modification of the propagation plane. The magnetic field-induced change of the electron oscillation momentum implies that the SPR energy also varies and hence the plasmon frequency shifts in the presence of an applied magnetic field [203]. When using circularly polarized light, circular plasmonic modes with right and left polarization are split in energy in presence of a magnetic field parallel to the propagation direction giving rise to MCD nearby the SPR [229] (Fig. 5.3 iv). Nowadays different Kerr, Faraday and MCD effects have been demonstrated in Au [231], Ag [232, 233] and even in plasmonic semiconductors [234, 235] on nanoparticles, discs, rods and other morphologies. The MO effect of plasmonics nanoparticles varies linearly with the magnetic field, and it requires strong magnetic fields to be significant [229, 236]. In fact, it is significantly smaller than that of magnetic materials due to their different electronic origin.

5.5 Perspectives

In previous chapters we showed several examples of the multifunctionality of the MP nanostructures. However, a wide number of difficulties must be overcome to obtain high performance MP materials and devices. Such difficulties are linked to the nature of the involved materials and to the difficulties in the chemical design of the researched morphologies. From the optical point of view, the large optical losses of the most investigated magnetic materials: magnetite and maghemite, and Fe, Co, Ni,

give rise to the damping of the plasmonic properties in the different nanostructures. Alternatively, more transparent magnetic materials, like magnetic garnets (YIG) or magnetic metal-doped semiconductors, like ferromagnetic Co doped ZnO [237] or paramagnetic CeF_3 [238] are known, but their synthesis as nanoparticles or similar is currently a challenge. In this case, a more promising design would be the synthesis of metallic multicomponent alloys, semiconductors or multicomponent oxides in which the optical, plasmonic and magnetic properties could be optimized thanks to the control of the composition. Also, the search of alternative plasmonic materials should be interesting to develop MP nanostructures, since the vastly employed Ag and Au are not fully optimal materials [10]. For example, even if Ag has low optical losses in the visible optical range, the nanoparticles are not stable as Ag oxidizes easily. Au is more chemically stable, but it has large losses. These metals have large absorption in the NIR region where many applications—like telecommunications (TC) and biomedicine—are now working. Strong research activity is currently focused on novel plasmonic materials [9] and the development of MP structures with these compounds will be interesting.

The previous question is crucial also for the development of MP-based magneto-optical devices. In fact, the magneto-optical figure of merit, i.e. the parameter that defines the efficiency of a material for MO applications, is inversely proportional to the absorption. Magnetic garnets and Eu-chalcogenides, that have smaller MO signal than Fe or Co metals, are however employed in optical telecom devices due to their small losses in the Vis and IR [14]. The synthesis of MP NPs with materials with better transparency, as was previously discussed, or the employment of magnetic materials with high MO properties as half-metallic or Heusler phases [240] holds great promise. However, the synthesis of nanoparticles of these materials has not been developed at the moment. An alternative is the design of single phase and hybrid MP NPs with a morphology in which MO and SPR signals are not directly coupled. For example, in asymmetric structures, like ellipsoidal discs, the main SPR and the plasmon MO resonance occurs at different energies as are correlated with different orientations of discs. As shown by Chen et al. [241] in ellipsoidal Ni discs or by Macaferri et al. [242] in ellipsoids while the optical SPR can be excited along the main axis of the ellipsoid, the plasmonic MO excitation occurs along the orthogonal short axis at different wavelength. On the other hand, similar gap between MO and SPR has been observed in 2D arrays in which a mixture of plasmonics (Au) and magnetic (Ni) discs are arranged. Depending on the relative orientation of light and the array structure, different dipolar coupling processes between the plasmonic and magnetic discs (Ni–Ni and Au–Ni) are possible [243, 244], giving rise to high MO signal in a low absorption regime. Theoretical studies show that the development of MP photonic crystals composed of mixtures or single NPs could give rise to high magneto-optical performances.

Directly correlated with MO effects is the use of MPs for magnetic storage technologies [245, 246]. Heat Assisted Magnetic Recording (HARM) [247] is a commercial technology that takes advantage of the interplay between magnetic and plasmonic units to reach record (2 Tb/in.^{2}) density of magnetic storage [248]. This technology employs ultrafast switching of the magnetization of bits thanks to the local heating

produced by plasmon induced confinement of light. This is obtained by coupling a plasmonic antenna to a continuous magnetic medium [197]. Alternatively, all-optical magnetic recording has also been proposed as an ultrafast technology in the THz regime to switching the magnetization in magnetic memory and logic spintronic devices [250–253]. Ultrafast and high-power laser pulses allow magnetic erasing and writing processes thanks to a phenomenon known as the inverse Faraday effect. The incorporation of plasmonic structures should enhance the EMFs while at the same time allowing subwavelength spatial resolution inverse Faraday effects [251, 254, 255] and hence facilitate the incorporation of this technology in the on-chip submicrometric devices. While these two technologies are now investigated in films, 3D dots will be the further progress technology—for example, heated dot magnetic recording (HDMR) promises up to 10 Tb/in.^{2} [256]. Some works have investigated the possibility of MO writing and reading employing MP multilayer dots [255]. Here the aim is to overcome the limit of magneto-optical imaging in terms of spatial resolution [246]. MP nanoparticles should be the prototypes to investigate future developments of these technologies.

While the former technology (HAMR) takes advantage of the heat-induced demagnetization process, a different type of photo-induced switching mechanism activated by plasmonic resonance was proposed in Bogani et al. [257]. In this study the MO-detected hysteresis loops of AuFe nanoparticles with high coercive field were measured under the simultaneous irradiation with low power light at different wavelengths. The authors observed a faster magnetic relaxation of the nanoparticles when irradiating at the SPR wavelength. Different tests excluded that the observed phenomena were due to plasmon induced thermal or inverse Faraday effects. The authors propose that spin scattering processes are activated by the plasmon-induced electronic excitations.

Another field in which the multifunctional capabilities of MP NPs are very attractive is that of biomedical applications [246]. The development of theranostic approaches, *i.e.* diagnostic, imaging and therapeutic capabilities on a single platform for efficient and personalized treatment of cancer and other diseases, is a field in which the combination of the different performances of the plasmonics and magnetic moieties of the MP NPs can bring significant momentum. The benefit is also the possibility of overcoming the natural limits of each technique: the red-shift of SPR of the MP NPs allows imaging and treatment using IR radiation, while radio frequency-induced hyperthermia allows to perform thermal therapy in deeper regions of the body, unreachable to light, or to increase local temperature combining magneto- and photo-thermia. First demonstrations have been shown [258]; however, one of the main limitations for these applications is the restriction to Au for plasmonic and Fe oxide for the magnetic moiety taking into account cytotoxicity criteria. On the other hand, Ag has a stronger and narrower SPR compared to Au, while the Co-ferrite or FeCo alloys have larger anisotropy and magnetization respectively than the Fe oxides. However, these better compounds are chemically unstable in the body and cytotoxic.

Currently, different plasmonic diagnostic and sensing devices or platforms, using LSPR effects, are under investigation. MP NPs are gathering interest due to the possibility to combine the plasmonic application and an improvement in the efficiency to separate, concentrate or localize the analyte thanks to magnetic control in such a way to increase the sensibility, selectivity and detection rate. On the other hand, MO effects are being considered for the detection method. Recently, MCD and Kerr effects have been demonstrated to be high performance techniques for optical sensing of non-magnetic plasmonic structures [229]. However, since the MO signal of the magnetic materials is larger than that of the plasmonic ones and it can be reached applying smaller magnetic fields, the performance of magnetic structures should be better. On the other hand, MO spectroscopy could be useful to improve the selectivity of optical detection. Taking advantage of the phase change of the MO signal near the SPR proposed in [259], Macaferri et al. [260] developed an ultrasensitive and label-free molecular-level detection using ellipsoidal Ni nanodiscs and Kerr effect detection.

The employment of MP nanostructures for optimizing catalytic processes is another interesting application for magnetic-plasmonic hybrid structures. Most of the investigations exploit the bifunctionality of these structures, using for instance the capability of magnetic concentration, or the functionalization of the plasmonic surface. However, new scenarios that benefit from the properties of these hybrid structures are becoming clear: in hybrid structures like Au@Fe-oxides, the charge transfer mechanism and the charge depletion region can modulate the surface charge for catalytic reactions [90, 261–263]. On the other hand, plasmon-mediated catalytic processes are activated thanks to the local heat induced at the resonance [137]. In the case of MP NPs, the combination of photothermal and magnetic induced hyperthermia can be a new approach for controlling catalytic processes.

Another interesting perspective regards spin-plasmonics, i.e. the effects correlated to the net spin-polarization of the electrons involved in the plasmonic excitations. The spin polarization of *s*-band should not occur in pure plasmonic materials since they are diamagnetic, while it occurs in the *s* and *d* bands at the Fermi lever of the magnetic metals. In these materials, the spin-unbalance of *s*-electrons at the Fermi level is much smaller than the one corresponding to localized *d*-electrons. Several experiments based on X-Ray Magnetic Circular Dichroism spectroscopy have demonstrated the possibility to magnetize plasmonic elements. This has been observed in MPs metallic alloy based nanoparticles, like in AuFe [26, 27] NPs, or in metal@oxide hybrid heterostructures like Au@Fe_3O_4 CS NPs [89] as previously discussed. In magnetic materials, different intrinsic and extrinsic spin scattering mechanisms can give rise to different magneto-transport effects which are the base of magnetoresistance sensors and other spintronic devices. The effects due to a spin population and the spin scattering process in the SPR resonance has not been considered at the moment.

The landscape of new effects and applications of Magneto-plasmonic materials that is progressively appearing shows an increasing crossover of the MP effects with thermal effects. Several cases were discussed above in which magnet/plasmon/thermal effects are correlated, in particular to the photothermal

and magnetic hyperthermia effects therapies and plasmon driven demagnetization process. However, other crossing mechanisms can be outlined. Martin et al. [264] theoretically showed that the spatial thermal diffusion of the plasmon-induced heat between MP nanoparticles can be controlled by the MO effects. Experiments by Temnov et al. [265, 266] demonstrate the modulation of the non-linear optical properties of propagating plasmons in magnetoplasmonic multilayers induced by the thermal process at the magnetic interfaces. In addition, in MP NPs, single phase or hybrid, phononic and magnonic excitations are affected, and coupled, by size effects of the moieties, the inter and intra particle coupling and by the particle morphology. The fact that an increasing number of novel properties are being observed in magnetic and plasmonic nanostructures using other external stimulus—like chirality light, electrical and electrochemical fields or mechanical forces—[14, 72, 171, 174, 197, 251] involves that MPs will be excellent benchmark materials to design and investigate multi-responsive, multifunctional nanomaterials.

Acknowledgements This work has been supported by the European Union's Horizon 2020 Research and Innovation program under Grant agreement No. 737093 (FEMTOTERABYTE https://www.physics.gu.se/femtoterabyte) and by the University of Pisa through project PRA_2017_25.

References

1. S.A. Maier, *Plasmonics: Fundamentals and Applications* (Springer, New York, 2007)
2. J.A. Schuller, E.S. Barnard, W. Cai, Y.C. Jun, J.S. White, M.L. Brongersma, Nat. Mater. **9**, 193 (2010)
3. D.K. Gramotnev, S.I. Bozhevolnyi, Nat. Photon. **4**, 83 (2010)
4. O. Tokel, F. Inci, U. Demirci, Chem. Rev. **114**, 5728 (2014)
5. J. Langer, S.M. Novikov, L.M. Liz-Marzán, Nanotechnology **26**, 322001 (2015)
6. U. Kreibig, M. Vollmer, *Optical Properties of Metal Cluster* (Springer, Berlin, 1995)
7. S.K. Ghosh, T. Pal, Chem. Rev. **107**, 4797 (2007)
8. M.A. García, J. Phys. D: Appl. Phys. **44**, 283001 (2011)
9. S. Kim, J.M. Kim, J.E. Park, J.M. Nam, Adv. Mater. **30**, 1704528 (2018)
10. B. Doiron, M. Mota, M.P. Wells, R. Bower, ACS Photon. **6**, 240 (2019)
11. J.M.D. Coey, *Magnetism and Magnetic Materials* (Cambridge University Press, New York, 2010)
12. G. Armelles, A. Cebollada, A. García-Martín and M. Ujué González, Adv. Opt. Mater. **1**, 10 (2013).
13. R. Scarfiello, C. Nobile, P.D. Cozzoli, Front. Mater. **3**, 1 (2016)
14. D. Floess, H. Giessen, Rep. Prog. Phys. **81**, 116401 (2018)
15. V.T. Tran, J. Kim, L.T. Tufa, S. Oh, J. Kwon, J. Lee, Anal. Chem. **90**, 225 (2018)
16. P.B. Johnson, R.W. Christy, Phys. Rev. B **6**, 4370 (1972)
17. P.B. Johnson, R.W. Christy, Phys. Rev. B **9**, 5056 (1974)
18. K.K. Tikuišis, L. Beran, P. Cejpek, K. Uhlírová, J. Hamrle, M. Vaňatka, M. Urbánek, M. Veis, Mater. Design. **114**, 31 (2017)
19. G. Armelles, D. Weller, B. Rellinghaus, R.F.C. Farrow, M.F. Toney, P. Caro, A. Cebollada, M.I. Alonso, IEEE Trans. Magn. **33**, 3419 (1997)
20. N.W. Ashcroft, N.D. Mermin, *Solid State Physics* (Saunders College, Philadelphia, 1976)

21. J.L. Menéndez, B. Bescós, G. Armelles, R. Serna J. Gonzalo, R. Doole, A.K. Petford-Long, M.I. Alonso, Phys. Rev. B **65**, 205413 (2002)
22. H. Amekura, Y. Takeda, N. Kishimoto, Nucl. Instr. Meth. Phys. Res. B **222**, 96 (2004)
23. C. Clavero, A. Cebollada, G. Armelles, Y. Huttel, Phys. Rev. B **72**, 024441 (2005)
24. S. Ozaki, H. Kura, H. Maki, T. Sato, J. Appl. Phys. **105**, 113913 (2009)
25. C.Y. You, Z.Q. Yang, Q.F. Xiao, I. Škorvánek, Eur. Phys. J. Appl. Phys. **28**, 73 (2004)
26. C. de Julián Fernández, G. Mattei, E. Paz, R.L. Novak, L. Cavigli, L. Bogani, F.J. Palomares, P. Mazzoldi, A. Caneschi, Nanotechnology **21**, 165701 (2010)
27. V. Amendola, M. Meneghetti, O.M. Bakr, P. Riello, S. Polizzi, D.H. Anjum, S. Fiameni, P. Arosio, T. Orlando, C. de Julián Fernández et al., Nanoscale **5**, 5611 (2013)
28. N. Chen, Di Wang, T. Feng, R.A. Kruk, Nanoscale **7**, 6607 (2015)
29. P. Srinoi, Y.T. Chen, V. Vittur, M.D. Marquez, T.R. Lee, Appl. Sci. **8**, 1106 (2018)
30. R. Ferrando, J. Jellinek, R.L. Johnston, Chem. Rev. **108**, 846 (2008)
31. H. Zeng, S. Sun, Adv. Func. Mater. **18**, 391 (2008)
32. F.H. Lin, R.A. Doong, J. Coll. Interf. Sci. **417**, 325 (2014)
33. L. Carbone, P.D. Cozzoli, Nano Today **5**, 449 (2010)
34. M.B. Cortie, A.M. McDonagh, Chem. Rev. **111**, 3713 (2011)
35. K.C.F. Leung, S. Xuan, X. Zhu, D. Wang, C.P. Chak, S.F. Lee, W.K.W. Hob, B.C.T. Chung, Chem. Soc. Rev. **41**, 1911 (2012)
36. T.T. Nguyen, F. Mammeri, S.A. Nguyen, Nanomaterials **8**, 149 (2018)
37. C.S. Levin, C. Hofmann, T.A. Ali, A.T. Kelly, ACS Nano **3**, 1379 (2009)
38. L. Wang, C. Clavero, Z. Huba, K.J. Carroll, E.E. Carpenter, D. Gu, R.A. Lukaszew, Nano Lett. **11**, 1237 (2011)
39. W. Brullot, V.K. Valev, T. Verbiest, Nanomed. NBM **8**, 559 (2012)
40. R. Sachan, A. Malasi, J. Ge, S. Yadavali, H. Krishna, ACS Nano **8**, 9790 (2014)
41. E.A. Chaffin, S. Bhana, R.T. O'Connor, X. Huang, Y. Wang, J. Phys. Chem. B **118**, 14076 (2014)
42. W.F.J. Fontijn, P.J. van der Zaag, M.A.C. Devillers, V.A.M. Brabers, R. Metselaar, Phys. Rev. B **56**, 5432 (1997)
43. V. Doormann, J.P. Krumme, H. Lenz, J. Appl. Phys. **68**, 3544 (1990)
44. W. Shi, H. Zeng, Y. Sahoo, T.Y. Ohulchanskyy, Nano Lett. **6**, 875 (2006)
45. V. Velasco, L. Muñoz, E. Mazarío, N. Menéndez, P. Herrasti, A. Hernando, P. Crespo, J. Phys. D Appl. Phys. **48**, 035502 (2015)
46. B. Wang, S. Qu, Appl. Surf. Sci. **292**, 1002 (2014)
47. M. Wang, C. Gao, L. He, Q. Lu, J. Zhang, C. Tang, S. Zorba, Y. Yin, J. Am. Chem. Soc. **135**, 15302 (2013)
48. E. Prodan, P. Nordlander, N.J. Halas, Chem. Phys. Lett. **368**, 94 (2003)
49. C. Radloff, N.J. Halas, J. Chem. Phys. **120**, 5444 (2004)
50. A. Mahmed, A. Mehaney, M. Shaban, A.H. Aly, Mater. Res. Express **6**, 085073 (2019)
51. A. López-Ortega, M. Takahashi, S. Maenosono, P. Vavassori, Nanoscale **10**, 18672 (2018)
52. G.V. Hartland, Chem Rev **111**, 3858 (2011)
53. Y. Li, Q. Qiang Zhang, A.V. Nurmikko, S. Sun, Nano Lett. **5**, 1689 (2005)
54. K. Korobchevskaya, C. George, A. Diaspro, L. Manna, R. Cingolani, A. Comin, Appl. Phys. Lett. **99**, 18 (2011)
55. K. Korobchevskaya, C. George, L. Manna, A. Comin, J. Phys. Chem. C **116**, 26924 (2012)
56. A. Comin, K. Korobchevskaya, C. George, A. Diaspro, Nano Lett. **12**, 921 (2012)
57. C. Caruntu, B.C. Cushing, G. Caruntu, C.J. O'Connor, Chem. Mater. **17**, 3398 (2005)
58. F. Carlà, G. Campo, C. Sangregorio, A. Caneschi, C. de Julián Fernández, L.I. Cabrera, J. Nanopart. Res. **15**, 1813 (2013)
59. I. Urries, C. Muñoz, L. Gomez, C. Marquina, V. Sebastián, M. Arruebo, J. Santamaria, Nanoscale **6**, 9230 (2014)
60. X. Hou, X. Wang, R. Liu, H. Zhang, X. Liu, X. Liu, Y. Zhang, RSC Adv. **7**, 18844 (2017)
61. E.V. Shevchenko, M.I. Bodnarchuk, M.V. Kovalenko, D.V. Talapin, Adv. Mater. **20**, 4323 (2008)

62. W. Chen, N. Xu, L. Xu, L. Wang, Z. Li, W. Ma, Y. Zhu, C. Xu, N.A. Kotov, Macromol. Rapid. Commun. **31**, 228 (2010)
63. Y. Jin, C. Jia, S.-W. Huang, M.O. 'Donnell, X. Gao, Nat. Commun. **1**, 41(2010)
64. H. Mohammad-Beigi, S. Yaghmaei, R. Roostaazad, A. Arpanaei, Physica E **49**, 30 (2013)
65. X. Jin, H. Li, S. Wang, N. Kong, H. Xu, Q. Fu, H. Gua, J. Ye, Nanoscale **6**, 14360 (2014)
66. E.D. Smolensky, M.C. Neary, Y. Zhou, T.S. Berquo, V.C. Pierre, Chem. Comm. **47**, 2149 (2011)
67. M. Zhang, D.J. Magagnosc, I. Liberal, Y. Yu, H. Yun, H. Yang, Y. Wu, J. Guo, W. Chen, Y.J. Shin, A. Stein, J.M. Kikkawa, N. Engheta, D.S. Gianola, C.B. Murray, C.R. Kagan, Nat. Nanotech. **12**, 228 (2017)
68. G. Campo, F. Pineider, E. Fantechi, C. Innocenti, A. Caneschi, C. de Julián Fernández, J Nanosci. Nanotechnol. **19**, 4946 (2019)
69. A.C. Templeton, J.J. Pietron, R.W. Murray, P. Mulvaney, J. Phys. Chem. B **104**, 564 (2000)
70. C.F. Bohren, D.P. Gilra, J. Coll. Interf. Sci. **72**, 215 (1979)
71. I.W. Sudiarta, P. Chylek, J. Opt. Soc. Am. **67**, 561 (2001)
72. N. Passarelli, L.A. Pérez, E.A. Coronado, ACS Nano **8**, 9723 (2014)
73. M. Xiong, X. Jin, J. Jian Ye, Nanoscale **8**, 4991(2016)
74. E.V. Shevchenko, D.V. Talapin, C.B. Murray, S. O'Brien, J. Am. Chem. Soc. **128**, 3620 (2006)
75. W. Brullot, R. Strobbe, M. Bynens, M. Bloemen, P.J. Demeyer, W. Vanderlinden, S. De Feyter, V.K. Valev, T. Verbiest, Mater. Lett. **118**, 99 (2014)
76. P. Crespo, R. Litrán, T.C. Rojas, M. Multigner, J.M. de la Fuente, J.C. Sánchez-López, M.A. García, A. Hernando, S. Penadés, A. Fernández, Phys. Rev. Lett. **93**, 087204 (2004)
77. G.L. Nealon, B. Donnio, R. Greget, J.P. Kappler, E. Terazzi, J.L. Gallani, Nanoscale **4**, 5244 (2012)
78. Y. Lee, M.A. García, N.A. Frey Huls, S. Sun, Angew. Chem. Int. Ed. **49**, 1271 (2010)
79. C. Wang, Y. Wei, H. Jiang, S. Sun, Nano Lett. **9**, 4544 (2009)
80. C. George, A. Genovese, F. Qiao, K. Korobchevskaya, Nanoscale **3**, 4647 (2011)
81. F. Vita, C. Innocenti, A. Secchi, F. Albertini, V. Grillo, A. Fiore, P.D. Cozzoli, C. de Julián Fernández, J. Mater. Chem. C (2018)
82. R.H. Kodama, A.E. Berkovitz, E.J. Mcni, S. Foner, Phys. Rev. Lett. **77**, 394 (1996)
83. K. Kachkachi, A. Ezzir, M. Nogués, E. Tronc, Eur. Phys. J. B **14**, 681 (2002)
84. C. Martínez-Boubeta, K. Simeonidis, M. Angelakeris, N. Pazos-Pérez, M. Giersig, A. Delimitis, L. Nalbandian, V. Alexandrakis, D. Niarchos, Phys. Rev. B **74**, 054430 (2006)
85. S. Chandra, N.A. Frey Huls, M.H. Phan, S. Srinath, M.A. García, Y. Lee, C. Wang, S. Sun, O. Iglesias, H. Srikanth, Nanotechnology **25**, 055702 (2014)
86. A. Luchini, G. Vitiello, F. Rossi, O. Ruiz de Ballesteros, A. Radulescu, G. D'Errico, D. Montesarchio, C. de Julián Fernández, L. Paduano, Phys. Chem. Chem. Phys. **17**, 6087 (2015)
87. L. Zhu, X. Deng, Y. Hu, J. Liu, Nanoscale **10**, 21499 (2018)
88. P. Tancredi, L. Souza da Costa, S. Calderón, O. Moscoso-Londoño, L. M. Socolovsky, P.J. Ferreira, D. Muraca, D. Zanchet, M. Knobel, Nano Res. **12**, 1781 (2019)
89. F. Pineider, C. de Julián Fernández, V. Videtta, E. Carlino, A. al Hourani, F. Wilhelm, A. Rogalev, P.D. Cozzoli, P. Ghigna, C. Sangregorio, ACS Nano **7**, 857 (2013)
90. M. Feygenson, J.C. Bauer, Z. Gai, C. Marques, M.C. Aronson, X. Teng, D. Su, V. Stanic, V.S. Urban, K.A. Beyer, S. Dai, Phys. Rev. B **92**, 054416 (2015)
91. M. Kim, H. Song, J. Mater Chem C **2**, 4997 (2014)
92. P. Guardia, S. Nitti, M.E. Materia, G. Pugliese, N. Yaacoub, J.-M. Greneche, C. Lefevre, L. Manna, T. Pellegrino, J. Mater. Chem. B **5**, 4587 (2017)
93. A. Pariti, P. Desai, S.K.Y. Maddirala, N. Ercal, K.V. Katti, X. Liang, M. Nath, Mater. Res. Express **1**, 035023 (2014)
94. M.E.F. Brollo, J.M. Orozco-Henao, R. López-Ruiz, D. Muraca, C.S.B. Dias, K.R. Pirota, M. Knobel, J. Magn. Magn. Mater. **397**, 20 (2016)
95. P. Tancredi, O. Moscoso Londoño, P.C. Rivas Rojas, U. Wolff, L.M. Socolovsky, M. Knobel, D. Muraca, J. Phys. D Appl. Phys. **51**, 295303 (2018)
96. N.A. Frey, S. Srinath, H. Srikanth, C. Wang, S. Sun, IEEE Trans. Magn. **43**, 3094 (2007)

97. J.G. Ovejero, I. Morales, P. de la Presa, N. Mille, J. Carrey, M.A. García, A. Hernando, P. Herrasti, Phys. Chem. Chem. Phys. **20**, 24065 (2018)
98. M. Knobel, W.C. Nunes, L.M. Socolovsky, E. De Biasi, J. Nanosci. Nanotechnol. **8**, 2836 (2008)
99. X. Batlle, A. Labarta, J. Phys. D: Appl. Phys. **35**, R15 (2002)
100. P. Singh, M. Shukla, C. Upadhyay, Nanoscale **10**, 22583 (2018)
101. N.A. Frey, N.H. Phan, H. Srikanth, S. Srinath, J. Appl. Phys. **105**, 07B502 (2009)
102. L. León-Félix, J. Chaker, M. Parise, J.A.H. Coaquira, Hyperfine Interact. **224**, 179 (2014)
103. M. Bozorth, *Ferromagnetism* (Van Nostrand, Toronto, 1951)
104. D.A. Gilbert, L.W. Wang, T.J. Klemmer, J.U. Thiele, C.H. Lai, K. Liu, Appl. Phys. Lett. **102**, 132406 (2013)
105. A.P. Murani, J. Phys. F Met. Phys. **4**, 757 (1974)
106. B. Verbeek, J. Mydosh, J. Phys. F Met. Phys. **8**, L109 (2001)
107. F. Wilhelm, P. Poulopoulos, V. Kapaklis, J.P. Kappler N. Jaouen, A. Rogalev, A.N. Yaresko, C. Politis, Phys. Rev. B **77**, 224414 (2008)
108. J.R. Childress, C.L. Chien, Phys. Rev. B **43**, 8089 (1991)
109. J. Noetzel, A. Handstein, A. Mucklich, F. Prockert, J. Magn. Magn. Mater. **205**, 183 (1999)
110. N. Jaouen, F. Wilhelm, A. Rogalev, J. Goulon, J. Phys. Condens. Matter **20**, 095005 (2008)
111. J. Bartolomé, L.M. García, F. Bartolomé, F. Luis, R. López-Ruiz, F. Petroff, C. Deranlot, F. Wilhelm, A. Rogalev, P. Bencok et al., Phys. Rev. B **77**, 184420 (2008)
112. C. Maurizio, N. Michieli, B. Kalinic, V. Mattarello, V. Bello, F. Wilhelm, K. Ollefs, G. Mattei, Appl. Surf. Sci. **433**, 596 (2018)
113. J.K. Lim, S.A. Majetich, Nano Today **8**, 98 (2013)
114. I. Schick, D. Gehrig, M. Montigny, B. Balke, M. Panthöfer, A. Henkel, F. Laquai, W. Tremel, Chem. Mater. **27**, 4877 (2015)
115. J. Canet-Ferrer, P. Albella, A. Ribera, J.V. Usagre, S.A. Maier, Nanoscale Horiz. **2**, 205 (2017)
116. Y. Song, V.T. Tran, J. Lee, A.C.S. Appl, Mater. Interf. **9**, 24433 (2017)
117. J. Zeng, M. Gong, D. Wang, M. Li, W. Xu, Z. Li, S. Li, D. Zhang, Z. Yan, Y. Yin, Nano Lett. **19**, 3011 (2019)
118. H. Wang, D.W. Brandl, F. Le, P. Nordlander, N.J. Halas, Nano Lett. **6**, 827 (2006)
119. Y. Chen, N. Gao, J. Jiang, Small **9**, 3242 (2013)
120. Z. Li, J.J. Foley IV., S. Peng, C.J. Sun, Y. Ren, G.P. Wiederrecht, S.K. Gray, Y. Sun, Angew. Chem. Int. Ed. **54**, 8948 (2015)
121. Z. Li, A. López-Ortega, A. Aranda-Ramos, J.L. Tajada, J. Sort, C. Nogues, P. Vavassori, J. Nogues, B. Sepúlveda, Small **14**, 1800868 (2018)
122. B.H. Jun, M.S. Noh, J. Kim, G. Kim, H. Kang, M.S. Kim, Y.T. Seo, J. Baek, J.H. Kim, J. Park, S. Kim, Y.K. Kim, T. Hyeon, M.H. Cho, D.H. Jeong, Y.S. Lee, Small **6**, 119 (2010)
123. X. Zhou, W. Xu, Y. Wang, Q. Kuang, Y. Shi, L. Zhong, Q. Zhang, J. Phys. Chem. C **114**, 19607 (2010)
124. A. Mezni, I. Imen Balti, A. Mlayah, N. Jouini, L.S. Smiri, J. Phys. Chem. C **117**, 16166 (2013)
125. C. Yuen, Q. Liu, Analyst **138**, 6494 (2013)
126. Z. Sun, J. Du, F. Duan, K. He, J. Mater. Chem. C **6**, 2252 (2018)
127. V. Amendola, S. Scaramuzza, S. Agnoli, S. Polizzi, M. Meneghetti, Nanoscale **6**, 1423 (2014)
128. V. Amendola, S. Scaramuzza, L. Litti, M. Meneghetti, Small **10**, 2476 (2014)
129. S. Scaramuzza, S. Polizzi, V. Amendola, Nanoscale Adv. **1**, 2681 (2019)
130. Y.H. Lim, M.Y. Cho, J.K. Kim, S. Hwangbo, B.H. Chung, ChemBioChem **8**, 2204 (2007)
131. R. Bardhan, W. Chen, M. Bartels, C. Pérez-Torres, M.F. Botero, R.W. McAninch, A. Contreras, R. Schiff, R.G. Pautler, N.J. Halas, A. Joshi, Nano Lett. **10**, 4920 (2010)
132. D.K. Kirui, D.A. Rey, C.A. Batt, Nanotechnology **21**, 105105 (2010)
133. S. Bhana, G. Lin, L. Wang, H. Starring, S.R. Mishra, G. Liu, X. Huang, A.C.S. Appl, Mater. Interf. **7**, 11637 (2015)
134. L. Huang, L. Ao, D. Hu, W. Wang, Z. Sheng, W. Su, Chem. Mater. **28**, 5896 (2016)
135. Z. Li, A. Aranda-Ramos, P. Güell-Grau, J.L. Tajada, L. Pou-Macayo, S. Lope Piedrafita, F. Pi, A.G. Roca, M.D. Baró, J. Sorte, et al., Appl. Mater. Today **12**, 430 (2018)

136. C. Multari, M. Miola, F. Laviano, R. Gerbaldo, G. Pezzotti, D. Debellis, E. Verné, Nanotechnology **30**, 255705 (2019)
137. Q. Ding, H. Zhou, H. Zhang, Y. Zhang, G. Wang, H. Zhao, J. Mater. Chem. A, **4**, 8866 (2016)
138. V.J. Pansare, S. Hejazi, W.J. Faenza, R.K. Prud'homme, Chem. Mater. **24**, 812 (2012)
139. B. Pelaz, C. Alexiou, R.A. Alvarez-Puebla, F. Alves, A.M. Andrews, S. Ashraf, L.P. Balogh, L. Ballerini, A. Bestetti, C. Brendel, S. Bosi et al., ACS Nano **11**, 2313 (2017)
140. N. Lewinski, V. Colvin, R. Drezek, Small **4**, 26 (2008)
141. B.R. Smith, S.S. Gambhir, Chem. Rev. **117**, 901 (2017)
142. D. Lombardo, M.A. Kiselev, M.T. Caccamo, J. Nanomater. 3702518 (2019). https://doi.org/10.1155/2019/3702518
143. L.H. Reddy, J.L. Arias, J. Nicolas, P. Couvreur, Chem. Rev. **112**, 5818 (2012)
144. Q. Feng, Y. Liu, J. Huang, K. Chen, J. Huang, K. Xiao, Sci. Rep. **8**, 2082 (2018)
145. J.T. Jenkins, D.L. Halaney, K.V. Sokolov, L.L. Ma, H.J. Shipley, S. Mahajan, C.L. Louden, R. Asmis, T.E. Milner, K.P. Johnston, M.D. Feldman, Nanomed. Nanotechn. Biol. Med. **9**, 356 (2013)
146. J. Kolosnjaj-Tabi, Y. Javed, L. Lartigue, J. Volatron, D. Elgrabli, I. Marangon, G. Pugliese, B. Caron, A. Figuerola, N. Luciani et al., ACS Nano **9**, 7925 (2015)
147. L. Li, S. Fu, C. Chen, X. Wang, C. Fu, S. Wang, W. Guo, X. Yu, X. Zhang, Z. Liu et al., ACS Nano **9**, 7094 (2016)
148. F. Mazuel, A. Espinosa, G. Radtke, M. Bugnet, S. Neveu, Y. Lalatonne, G.A. Botton, A. Abou-Hassan, C. Wilhelm, Adv. Funct. Mater. **27**, 1605997 (2017)
149. J.K. Lim, C. Lanni, E.R. Evarts, F. Lanni, R.D. Tilton, S.A. Majetich, ACS Nano **5**, 217 (2011)
150. E. Lueshen, I. Venugopal, J. Kanikunnel, T. Soni, Future Med. (2013). https://doi.org/10.2217/nnm.13.69
151. H. Zhou, F. Zou, K. Koh, J. Lee, J. Biomed. Nanotechnol. **10**, 2921 (2014)
152. X. Jin, H. Yu, N. Kong, J. Chang, H. Li, J. Ye, J. Mater. Chem. B **3**, 7787 (2015)
153. H.L. Liu, C.H. Sonn, J.H. Wu, K.M. Lee, Y.K. Kim, Biomaterials **29**, 4003 (2008)
154. Y.H. Bai, J.Y. Li, J.J. Xu, H.Y. Chen, Analyst **135**, 1672 (2010)
155. J. Li, Q. Xu, X. Wei, Z. Hao, J. Agric. Food Chem. **61**, 1435 (2013)
156. C.S. Bell, R. Mejías, S.E. Miller, J.M. Greer, M.S. McClain, T.L. Cover, T.D. Giorgio, ACS Appl. Mater. Interf. **9**, 26719 (2017)
157. R. Tavallaie, J. McCarroll, M. Le Grand, N. Ariotti, W. Schuhmann, E. Bakker, R.D. Tilley, D.B. Hibbert, M. Kavallaris, J.J. Gooding, Nat. Nanotech. **13**, 1066 (2018)
158. C. Xu, J. Xie, D. Ho, C. Wang, N. Kohler, N. Kohler, E.G. Walsh, J.R. Morgan, Y.E. Chin, S. Sun, Angew. Chem. Int. Ed. **47**, 173 (2008)
159. H. Jaganathan, R.L. Gieseck, A. Ivanisevic, J. Phys. Chem. C **114**, 22508 (2010)
160. E. Umut, F. Pineider, P. Arosio, C. Sangregorio, M. Corti, F. Tabak, A. Lascialfari, P. Ghigna, J. Magn. Magn. Mater. **324**, 2373 (2012)
161. T. Orlando, A. Capozzi, E. Umut, L. Bordonali, M. Mariani, P. Galinetto, F. Pineider, C. Innocenti, P. Masala, F. Tabak, M. Scavini, P. Santini, M. Corti, C. Sangregorio et al., J. Phys. Chem. C **119**, 1224 (2015)
162. F. Sousa, B. Sanavio, A. Saccani, Y. Tang, I. Zucca, T.M. Carney, A. Mastropietro, P.H.J. Jacob Silva, R.P. Carney, K. Schenk, et al., Bioconjugate Chem. **28**, 161 (2017)
163. J. Li, B. Arnal, C.W. Wei, J. Shang, M. O'Donnell, X. Gao, ACS Nano **9**, 1964 (2015)
164. J.G. Ovejero, S.J. Yoon, J. Li, A. Mayoral, X. Gao, M. O'Donnell, M.A. García, P. Herrasti, A. Hernando, Microchim. Acta **185**, 130 (2018)
165. G.A. Sotiriou, M.A. Visbal-Onufrak, A. Teleki, E.J. Juan, Chem. Mater. **25**, 4603 (2013)
166. R. Di Corato, A. Espinosa, L. Lartigue, M. Tharaud, S. Chat, T. Pellegrino, C. Ménager, F. Gazeau, C. Wilhelm, Biomaterials **35**, 6400 (2014)
167. F. Mohammad, G. Balaji, A. Weber, R.M. Uppu, Z. Sheng, W. Su, J. Phys. Chem. C **114**, 19194 (2010)
168. E. Fantechi, P.M. Castillo, E. Conca, F. Cugia, C. Sangregorio, M.F. Casula, Interface Focus **6**, 20160058 (2016)

169. D.H. Kim, E.A. Rozhkova, I.V. Ulasov, S.D. Bader, T. Rajh, M.S. Lesniak, V. Novosad, Nat. Mater. **9**, 169 (2010)
170. S. Leulmi, X. Chauchet, M. Morcrette, G. Ortiz, H. Joisten, P. Sabon, T. Livache, Y. Hou, M. Carrière, S. Lequiena, B. Dieny, Nanoscale **7**, 15904 (2015)
171. N. Jiang, X. Zhuo, J. Wang, Chem. Rev. **118**, 3054 (2018)
172. G. Armelles, A. Cebollada, A. García-Martín, J. García-Martín, M.U. González, J.B. González-Díaz, E. Ferreiro-Vila, J.F. Torrado, J. Opt. A Pure Appl. Opt. **11**, 114023 (2009)
173. V. Temnov, G. Armelles, U. Woggon, D. Guzatov, A. Cebollada, A. García-Martín, J.M. García-Martín, T. Thomay, A. Leitenstorfer, R. Bratschitsch, Nat. Photon. **4**, 107 (2010)
174. D. Bossini, V.I. Belotelov, A.K. Zvezdin, A.N. Kalish, A.V. Kimel, ACS Photon. **38**, 1385 (2016)
175. Q. Wei, H.M. Song, A.P. Leonov, J.A. Hale, D. Oh, Q.K. Ong, K. Ritchie, A. Wei, J. Am. Chem. Soc. **131**, 9728 (2009)
176. H.M. Song, Q. Wei, Q.K. Ong, A. Wei, ACS Nano **4**, 5163 (2010)
177. A. Tomitaka, H. Arami, Z. Huang, A. Raymond, E. Rodriguez, Y. Cai, M. Febo, Y. Takemura, M. Nair, Nanoscale **10**, 184 (2018)
178. W.P. Li, P.Y. Liao, C.H. Su, C.S. Yeh, J. Am. Chem. Soc. **136**, 10062 (2014)
179. W. Shi, X. Liu, C. Wei, Z. J. Xu, S. S. Wei Sim, L. Liu, C. Xu, Nanoscale **7**, 17249 (2015)
180. R. Di Corato, G. Béalle, J. Kolosnjaj-Tabi, A. Espinosa, O. Clément, A.K.A. Silva, C. Ménager, C. Wilhelm, ACS Nano **9**, 2904 (2015)
181. E. Cazares-Cortes, S. Cabana, C. Boitard, E. Nehlig, Adv. Drug Deliv. Rev. **138**, 233 (2019)
182. A. Espinosa, M. Bugnet, G. Radtke, S. Neveu, G.A. Botton, C. Wilhelm, A. Abou-Hassan, Nanoscale **7**, 18872 (2015)
183. A. Espinosa, R. Di Corato, J. Kolosnjaj-Tabi, P. Flaud, T. Pellegrino, C. Wilhelm, ACS Nano **10**, 2436 (2016)
184. M. Carril, I. Fernández, J. Rodríguez, I. García, S. Penadés, Part. Part. Syst. Charact. **31**, 81 (2014)
185. J. Zhu, Y. Lu, Y. Li, J. Jiang, Nanoscale **6**, 199 (2014)
186. T.H. Shin, Y. Choi, S. Kim, J. Cheon, Chem. Soc. Rev. **44**, 4501 (2015)
187. S.S. Kelkar, T.M. Reineke, Bioconj. Chem. **22**, 1879 (2011)
188. H. Kang, S. Hu, M.H. Cho, S.H. Hong, Y. Choi, H.S. Choi, Nano Today **23**, 59 (2018)
189. J. Lee, J. Yang, H. Ko, S.J. Oh, J. Kang, J. Kang, J.H. Son, K. Lee, S.W. Lee, H.G. Yoon, J.-S. Suh et al., Adv. Funct. Mater. **18**, 258 (2008)
190. L.S. Lin, X. Yang, Z. Zhou, Z. Yang, O. Jacobson, Y. Liu, A. Yang, G. Niu, J. Song, H.H. Yang, X. Chen, Adv. Mater. **29**, 1606681 (2017)
191. Z. Abed, J. Beik, S. Laurent, N. Eslahi, T. Khani, E.S. Davania, H. Ghaznavi, A. Shakeri-Zadeh, J. Cancer Res. Clin. Oncol. **145**, 1213 (2019)
192. M.V. Efremova, V.A. Naumenko, M. Spasova, A.S. Garanina, M.A. Abakumov, A.D. Blokhina, P.A. Melnikov, A.O. Prelovskaya, M. Heidelmann, Z.-A. Li et al., Sci. Rep. **8**, 11295 (2018)
193. M.V. Efremova, Y.A. Nalench, E. Myrovali, A.S. Garanina, I.S. Grebennikov, P.K. Gifer, M.A. Abakumov, M. Spasova, M. Angelakeris, A.G. Savchenko et al., Beilstein J. Nanotechnol. **9**, 2684 (2018)
194. A.K. Zvezdin, V.A. Kotov, *Modern Magnetooptics and Magnetooptical Materials* (IOP Publishing Ltd., Bristol, 1997)
195. P.M. Oppeneer in *Handbook of Magnetic Materials*, vol. 13, ed. by K.H.J. Buschow (Elsevier Science, 2001)
196. P. Oppeneer, V. Antonov, in *Spin-Orbit-Influenced Spectroscopies of Magnetic Solids*, eds. by H. Ebert, G. Schütz (Springer, Berlin/Heidelberg, 1996), p. 29
197. N. Maccaferri, J. Opt. Soc. Am. B **36**, E112 (2019)
198. H. Feil, C. Haas, Phys. Rev. Lett. **58**, 65 (1987)
199. D. Lacoste, B.A. Tiggelen, G.L.J.A. Rikken, A. Sparenberg, J. Opt. Soc. Am. A **15**, 1636 (1998)
200. J.S. Ahn, K.H. Kim, T.W. Noh, D.H. Riu, K.H. Boo, H.E. Kim, Phys. Rev. B **52**, 15244 (1995)

201. M. Abe, T. Suwa, Phys. Rev. B **70**, 235103 (2004)
202. P.H. Lissberger, P.W. Saunders, Thin Solid Films **34**, 323 (1976)
203. B. Sepúlveda, J.B. González-Díaz, A. García-Martín, L.M. Lechuga, G. Armelles, Phys. Rev. Lett. **104**, 147401 (2010)
204. J.B. González-Díaz, B. Sepúlveda, A. García-Martín, G. Armelles, Appl. Phys. Lett. **97**, 043114 (2010)
205. A. Bourzami, O. Lenoble, C. Féry, J.F. Bobo, M. Piecuch, Phys. Rev. B **59**, 11489 (1999)
206. L. Fernández García, C. Pecharromán, A. Esteban-Cubillo, P. Tiemblo, N. García, J.L. Menéndez, J. Nanopart. Res. **15**, 2119 (2013)
207. A. Miles, Y. Gai, P. Gangopadhyay, X. Wang, R.A. Norwood, J.J. Watkins, Opt. Mater. Express. **7**, 2126 (2017)
208. B. Kalska, J.J. Paggel, P. Fumagalli, M. Hilgendorff, M. Giersig, J. Appl. Phys. **92**, 7481 (2002)
209. C. Clavero, B. Sepúlveda, G. Armelles, Z. Konstantinović, M. García del Muro, A. Labarta, X. Batlle, J. Appl. Phys. **100**, 074320 (2006)
210. B. Kalska, K. Schwinge, J. Paggel, P. Fumagalli, M. Hilgendorff, M. Giersig, J. Appl. Phys. **98**, 044318 (2005)
211. C. Clavero, G. Armelles, J. Margueritat, J. Gonzalo, M. García del Muro, A. Labarta, X. Batlle, Appl. Phys. Lett. **90**, 182506 (2007)
212. D. Martín-Becerra, J.M. García-Martín, Y. Huttel, G. Armelles, J. Appl. Phys. **117**, 053101 (2015)
213. O. Vlasin, O. Pascu, A. Roig, G. Herranz, Phys. Rev. Appl. **2**, 054003 (2014)
214. P. Varytis, N. Stefanou, A. Christofi, N. Papanikolaou, J. Opt. Soc. Am. B **32**, 1063 (2015)
215. P. Varytis, P.A. Pantazopoulos, N. Stefanou, Phys. Rev. B **93**, 214423 (2016)
216. B. Toal, M. McMillen, A. Murphy, W. Hendren, M. Arredondo, R. Pollard, Nanoscale **6**, 12905 (2014)
217. G. Shemer, G. Markovich, J. Phys. Chem. B **106**, 9195 (2002)
218. S. Tomita, T. Kato, S. Tsunashima, S. Iwata, M. Fujii, S. Hayashi, Phys. Rev. Lett. **96**, 167402 (2006)
219. R. Fujikawa, A.V. Baryshev, J. Kim, H. Uchida, M. Inoue, J. Appl. Phys. **103**, 07D301 (2008)
220. A.V. Baryshev, H. Uchida, M. Inoue, J. Opt. Soc. Amer. B **30**, 2371 (2013)
221. Y. Li, Q. Zhang, A.V. Nurmikko, S. Sun, Nano Lett. **5**, 1689 (2005)
222. P.K. Jain, Y. Xiao, R. Walsworth, A.E. Cohen, Nano Lett. **9**, 1644 (2009)
223. R.K. Dani, H. Wang, S.H. Bossmann, G. Wysin, J. Chem. Phys. **135**, 224502 (2011)
224. F.E. Moolekamp III., K.L. Stokes, IEEE Trans. Magn. **45**, 4888 (2009)
225. M. Caminale, L. Anghinolfi, E. Magnano, F. Bondino, A.C.S. Appl, Mater. Interf. **5**, 1955 (2013)
226. D. Smith, K.L. Stokes, Opt. Express **14**, 5746 (2006)
227. P. Pineider, E. Pedrueza-Villalmanzo, M. Serri, A.M. Adamu, E. Smetanina, V. Bonanni, G. Campo, L. Poggini, M. Mannini, C. de Julián Fernández, et al., Mater. Horiz. **6**, 1148 (2019)
228. M.A. Zaitoun, W.R. Mason, C.T. Lin, J. Phys. Chem. B **105**, 6780 (2001)
229. F. Pineider, G. Campo, V. Bonanni, C. de Julián Fernández, G. Mattei, A. Caneschi, D. Gatteschi, C. Sangregorio, Nano Lett. **13**, 4785 (2013)
230. P. Haefnere, E. Luck, E. Mohle, Phys. Stat. Sol. B **185**, 289 (1994)
231. B. Han, X. Gao, L. Shi, Y. Zheng, K. Hou, J. Lv, J. Guo, W. Zhang, Z. Tang, Nano Lett. **17**, 6083 (2017)
232. Y. Ishikawa, H. Yao, Chem. Phys. Lett. **609**, 93 (2014)
233. T. Shiratsu, H. Yao, Phys. Chem. Chem. Phys. **20**, 4269 (2018)
234. A.V. Malakhovskiia, A.E. Sokolova, A.S. Tsipotan, S.M. Zharkova, V.N. Zabluda, Phys. Lett. A **382**, 980 (2018)
235. P. Yin, Y. Tan, H. Fang, M. Hegde, P.V. Radovanovic, Nat. Nanotechnol. **13**, 463 (2018)
236. G. Weick, D. Weinmann, Phys. Rev. B **83**, 125405 (2011)
237. G. Varvaro, A. Di Trolio, A. Polimeni, A. Gabbani, F. Pineider, C. de Julián Fernández, G. Barucca, P. Mengucci, A. Bonapasta, A.M. Testa, J. Mater. Chem. C **7**, 78 (2019)

238. P. Molina, V. Vasyliev, E.G. Víllora, K. Shimamura, Opt. Express **19**, 11786 (2011)
239. J.F. Dillon, J. Appl. Phys. **39**, 922 (1968)
240. T. Graf, C. Felser, S.S.P. Parkin, Prog. Solid State Chem. **39**, 1 (2011)
241. J. Chen, P. Albella, Z. Pirzadeh, P. Alonso-González, Florian Huth, S. Bonetti, V. Bonanni, J. Åkerman, J. Nogués, P. Vavassori, et al., Small **7**, 2341 (2011)
242. N. Maccaferri, J.B. González-Díaz, S. Bonetti, A. Berger, M. Kataja, S. van Dijken, J. Nogués, V. Bonanni, Z. Pirzadeh, A. Dmitriev et al., Opt. Expr. **21**, 9875 (2013)
243. M. Kataja, T.K. Hakala, A. Julku, M.J. Huttunen, S. van Dijken, P. Törmä, Nat. Commun. **6**, 7072 (2015)
244. M. Kataja, S. Pourjamal, N. Maccaferri, P. Vavassori, T.K. Hakala, M.J. Huttunen, P. Törmä, S. van Dijken, Opt. Exp. **24**, 3652 (2016)
245. R.L. Stamps, S. Breitkreutz, J. Åkerman, A. Chumak, Y.C. Otani, G.E.W. Bauer, J.U. Thiele, M. Bowen, S.A. Majetich, M Kläui, et al., J. Phys. D Appl. Phys. **47**, 333001 (2014)
246. D. Sander, S.O. Valenzuela, D. Makarov, C.H. Marrows, E.E. Fullerton, P. Fischer, J. McCord, P. Vavassori, S. Mangin, P. Pirro et al., J. Phys. D Appl. Phys. **50**, 363001 (2017)
247. W.A. Challener, C. Peng, A.V. Itagi, D. Karns, W. Peng, Y. Peng, X. Yang, X. Zhu, N.J. Gokemeijer, Y.-T. Tsia et al., Nature Photon. **3**, 220 (2009)
248. E. Gage, K.Z. Gao, J.G. Zhu, in *Energy-Assisted Magnetic Recording, Ultrahigh-Density Magnetic Recording, Storage Materials and Media Designs,* ed. by G. Varvaro, F. Casoli (Pan Stanford Publishing, Singapore, 2016), Chap. 4
249. B.C. Stipe, T.C. Strand, C.C. Poon, H. Balamane, T.D. Boone, J.A. Katine, J.-L. Li, V. Rawat, H. Nemoto, A. Hirotsune, O. Hellwig, et al., Nature Phot. **4**, 484 (2010)
250. C.D. Stanciu, F. Hansteen, A.V. Kimel, A. Kirilyuk, A. Tsukamoto, A. Itoh, Th. Rasing, Phys. Rev. Lett. **99**, 47601 (2007)
251. I.S. Maksymov, Nanomaterials **5**, 577 (2015)
252. J. Walowski, M. Münzenberg, J. Appl. Phys. **120** 140901 (2016)
253. A.L. Chekhov, A.I. Stognij, T. Satoh, T.V. Murzina, I. Razdolski, A. Stupakiewicz, Nano Lett. **18** 2970 (2018)
254. T.M. Liu, T. Wang, A.H. Reid, M. Savoini, B. Koene, P. Granitzka, C.E. Graves, D.J. Higley, Z. Chen, G. Razinskas et al., Nano Lett. **15**, 6862 (2015)
255. A. Dutta, A.V. Kildishev, V.M. Shalaev, A. Bolasseva, R.E. Marinero, Opt. Mater. Express **7** 4317 (2017)
256. https://www.kitguru.net/components/hard-drives/anton-shilov/seagate-demos-hamr-hdds-vows-to-start-commercial-shipments-in-late-2017.
257. L. Bogani, L. Cavigli, C. de Julián Fernández, P. Mazzoldi, G. Mattei, M. Gurioli, M. Dressel, D. Gatteschi, Adv. Mater. **22**, 4054 (2010)
258. H. Hao Yan, W. Shang, X. Sun, L. Zhao J. Wang, Z. Xiong, J. Yuan, R. Zhang, Q. Huang, K. Wang, et al., Adv. Func. Mater. **28**, 1705710 (2018)
259. V. Bonanni, S. Bonetti, T. Pakizeh, Z. Pirzadeh, J. Chen, J. Nogués, P. Vavassori, O.R. Hillenbrand, J. Åkerman, A. Dmitriev, Nano Lett. **11**, 5333 (2011)
260. N. Maccaferri, E. Keith. K.E. Gregorczyk, T.V.A.G. de Oliveira, M. Kataja, S. van Dijken, Z. Pirzadeh, A. Dmitriev, J. Åkerman, M. Knez, P. Vavassori, Nature Comm. **6**, 6150 (2015)
261. S. Liu, S. Q Bai, Y. Zheng, K. Wei Shah, M.-Y. Han, ChemCatChem **4**, 1462 (2012)
262. L. Shang, Y. Liang, M. Li, G.I.N. Waterhouse, P. Tang, D. Ma, L.Z. Wu, C.H. Tung, T. Zhang, Adv. Func. Mater. **27**, 1606215 (2017)
263. S. Sarveena, D. Muraca, P. Mendoza Zélis, Y. Javed N. Ahmad, J.M. Vargas, O. Moscoso-Londoño, M. Knobel, M. Singha, S.K. Sharma, RSC Adv. **6**, 70394 (2016)
264. R.M.A. Ekeroth, A. García-Martín, J.C. Cuevas, Phys. Rev. B **95**, 235428 (2017)
265. V.V. Temnov, Nat. Photon. **6**, 728 (2012)
266. V.V. Temnov, I. Razdolski, T. Pezeril, D. Makarov, D. Seletskiy, A. Melnikov, K.A. Nelson, J. Opt. **18**, 093002 (2016)